

# **Interference Potential of Ultrawideband Signals**

## **Part 1: Procedures to Characterize Ultrawideband Emissions and Measure Interference Susceptibility of C-band Satellite Digital Television Receivers**

**Michael Cotton  
Robert Achatz  
Jeffery Wepman  
Brent Bedford**



**U.S. DEPARTMENT OF COMMERCE  
Carlos M. Gutierrez, Secretary**

Michael D. Gallagher, Assistant Secretary  
for Communications and Information

February 2005



## **DISCLAIMER**

Certain commercial equipment, instruments, or materials are identified in this report to specify the technical aspects of the reported results. In no case does such identification imply recommendation or endorsement by the National Telecommunications and Information Administration, nor does it imply that the material or equipment identified is necessarily the best available for the purpose.



# CONTENTS

	Page
1. INTRODUCTION .....	1
1.1. Purpose and Approach of This Study .....	2
1.2. Organization of This Report .....	3
2. INTERFERENCE SIGNALS .....	4
2.1. Signal Description .....	4
2.1.1. Direct-Sequence Ultrawideband .....	4
2.1.2. Dithered-Pulse Ultrawideband .....	6
2.1.3. Multi-Band OFDM Ultrawideband .....	7
2.1.4. Gated Gaussian Noise .....	9
2.2. Computer Simulation .....	10
2.2.1. Reduction of System Complexity .....	10
2.2.2. Reduction of Samples .....	12
2.3. Implementation on the Vector Signal Generator .....	13
3. INTERFERENCE CHARACTERIZATION MEASUREMENTS .....	14
3.1. Metrics and Data Needed to Compute Them .....	14
3.2. Description of Test and Measurement Equipment .....	14
3.2.1. Vector Signal Analyzer .....	14
3.2.2. Spectrum Analyzer .....	16
3.2.3. Digital Oscilloscope .....	17
3.2.4. Power Meter .....	18
4. VICTIM RECEIVER .....	19
4.1. Satellite Digital Television Description .....	19
4.1.1. MPEG-2 Encoder .....	19
4.1.2. Forward Error Correction and Modulation .....	19
4.1.3. Receiver .....	20
4.2. DTV Quality Metrics .....	21
4.3. Operational Scenario Chosen for DTV Interference Susceptibility Tests .....	22
4.4. Satellite Signal Simulation .....	23
5. INTERFERENCE SUSCEPTIBILITY TESTS .....	24
5.1. Methodology .....	24
5.2. Test System .....	24
5.3. Procedures .....	26
5.3.1. Calibration .....	26
5.3.2. DTV Quality Metric Acquisition .....	26
6. SUMMARY .....	27
7. ACKNOWLEDGMENTS .....	28
8. REFERENCES .....	29

APPENDIX A: MATHEMATICAL SIGNAL DESCRIPTION.....	31
A.1. Direct-Sequence Ultrawideband.....	31
A.2. Dithered-Pulse Ultrawideband.....	32
A.3. Multi-Band OFDM Ultrawideband .....	33
A.4. Gated Gaussian Noise.....	35
APPENDIX B: VECTOR SIGNAL GENERATOR OPERATION .....	36
B.1. Operation in the Dual AWG Mode.....	36
B.2. Techniques to Optimize RF Output Performance.....	37
B.3. Waveform Conditioning .....	39
B.4. Operating Procedures.....	40
APPENDIX C: EFFECTS OF VSG LO FEED-THROUGH ON DTV INTERFERENCE SUSCEPTIBILITY TESTS .....	41
C.1. LO Feed-Through Inherent to DTV Systems .....	41
C.2. Experiment.....	43
C.3. Results.....	44
C.4. Effect of VSG LO Feed-Through on Carrier-Suppression Ratio.....	46
C.5. Conclusion .....	47
APPENDIX D: ESTIMATING AND GRAPHING THE AMPLITUDE PROBABILITY DISTRIBUTION OF COMPLEX-BASEBAND SIGNALS.....	48
D.1. Estimating the APD .....	48
D.2. Plotting the APD.....	49
D.3. Testing the Routines .....	50
D.4. Additional Comments.....	50
D.5. MATLAB Code.....	52
APPENDIX E: DYNAMIC RANGE OF THE VECTOR SIGNAL ANALYZER.....	54
E.1. Dynamic Range Measurement .....	54
E.2. Average Power Measurements of Fundamental Signals.....	54
E.3. APD Measurements of Fundamental Signals.....	55
E.4. Conclusion.....	55
APPENDIX F: TEST SYSTEM CHARACTERIZATION.....	61
F.1. Characterization of the Signal Paths.....	61
F.2. Dynamic Range of Interference Signal Path Cascaded with the VSA .....	63
F.3. Intermodulation Products in Satellite Signal Generator.....	63
APPENDIX G: HARDWARE SPECIFICATION.....	66
G.1. Interference Generation Subsystem.....	66
G.2. Calibration Subsystem/Test and Measurement Equipment .....	67
G.3. Satellite Simulation Subsystem .....	68
G.4. Coupling Subsystem.....	70
G.5. Receiver Subsystem.....	71
APPENDIX H: GLOSSARY .....	72

# INTERFERENCE POTENTIAL OF ULTRAWIDEBAND SIGNALS

## PART 1: PROCEDURES TO CHARACTERIZE ULTRAWIDEBAND EMISSIONS AND MEASURE INTERFERENCE SUSCEPTIBILITY OF C-BAND SATELLITE DIGITAL TELEVISION RECEIVERS

Michael Cotton, Robert Achatz, Jeffery Wepman, and Brent Bedford<sup>1</sup>

In this study, we hypothesize that ultrawideband (UWB) interference potential can be quantified in terms of UWB signal characteristics. To test this hypothesis, a test system was designed and built to inject UWB signals with known characteristics into a C-band satellite digital television receiver and quantitatively measure interference susceptibility via signal quality metrics (e.g., segment error rate, pre-Viterbi bit error rate, and modulation error ratio) taken from various points in the receiver signal processing chain. UWB signals are characterized by the amplitude probability distribution and power spectral density. Characterization measurements done with a vector signal analyzer provide amplitude and phase information to enable extensive post-measurement capability. This report describes the test setup and procedures in detail. Subsequent reports will provide assessment of interference potential for gated Gaussian noise bursts (Part 2) and modern UWB systems (Part 3).

Key words: digital television; interference; satellite communications; ultrawideband

### 1. INTRODUCTION

In April 2002, the Federal Communications Commission (FCC) released *FCC 02-48* [1] legalizing intentional, low-power UWB emissions between 3.1 GHz and 10.6 GHz for communications devices operated indoors. UWB emissions were limited to -41 dBm average power in 1-MHz bandwidth and 0 dBm peak power in 50-MHz bandwidth, where average power is measured over a 1-millisecond integration time. Related compliance measurements require continuous transmissions during the measurement period. The rules define a UWB device as one that emits signals with 10-dB bandwidth greater than 500 MHz or greater than 20% of the center frequency. The FCC rules do not specify how the bandwidth requirement is achieved, consequently allowing industry considerable breadth in choosing a modulation.

This breadth is exemplified by the development of Direct-Sequence (DS-UWB) and Multi-Band Orthogonal Frequency-Domain Multiplexing (MB-OFDM) ultrawideband technologies. Proponents of DS-UWB and MB-OFDM both seek standardization from IEEE (Institute of Electrical and Electronics Engineers) 802.15 working group 3a on high-rate (greater than 20 million bits per second) Wireless Personal Area Networks (WPAN). As the name implies,

---

<sup>1</sup> The authors are with the Institute for Telecommunication Sciences, National Telecommunications and Information Administration, U.S. Department of Commerce, Boulder, Colorado 80305.

WPAN is intended for short-distance (nominally less than 10 meters) wireless networking of devices such as PCs, personal digital assistants, digital cameras, and mobile phones.

Both DS-UWB and MB-OFDM transmitters are based on state-of-the-art integrated circuitry. DS-UWB modulation controls pulse polarity and hence supports phase shifting modulations. It achieves its ultra-wide bandwidth by transmitting sufficiently narrow pulses. MB-OFDM simultaneously modulates 122 carriers spaced 4.125 MHz apart to achieve its ultra-wide bandwidth and frequency hops the modulated carriers between non-overlapping bands.

Since previous work performed at the Institute for Telecommunication Sciences (ITS) [2 - 5] did not specifically look at susceptibility of receivers to DS-UWB or MB-OFDM emissions, and since there is little published information regarding their interference potential, ITS entered into a Cooperative Research and Development Agreement (CRADA) with the Freescale subsidiary of Motorola, Inc. to study how interference potential of these emissions could be quantified in terms of signal characteristics that distinguish UWB signals.

### **1.1. Purpose and Approach of This Study**

The purpose of this study is to provide data needed to predict the interference potential of various UWB signals. Results will be useful for regulatory agencies that are currently charged with defining UWB emission limits and corresponding compliance measurement procedures. Results will also be useful to the ultrawideband communications industry, which will only thrive if compliance measurement procedures fairly evaluate interference potential of all UWB signals.

Our approach is to inject carefully characterized interference into an operating narrowband receiver and measure susceptibility of the receiver with precisely defined signal quality metrics. Data will then be analyzed to determine if there are common signal characteristics that predict interference potential.

The victim receiver chosen for this interference susceptibility test is C-band satellite digital television (DTV). This receiver demodulates signals transmitted in the 3.7 to 4.2 GHz frequency range, which lies within the band allocated for UWB devices. We chose to generate the satellite signal in the laboratory rather than use an unpredictable live signal, to generate interference signals with a vector signal generator rather than rely solely on prototype devices, and to perform signal and system characterization measurements primarily with the vector signal analyzer to provide comprehensive data capable of being post-processed in many ways.

This study has been broken down into three parts whose results will be published in three separate reports. The first report provides procedures to generate and characterize various interference signals and measure the susceptibility of a satellite DTV victim receiver to these signals. It provides sufficient detail to allow for thorough review and replication of the test. The third report will present results for various UWB signals, which will include MB-OFDM, DS-UWB, and conventional pulse-position modulated pulses.

The second report will present results for gated-noise interference. In August 2004, the MB-OFDM Alliance Special Interest Group (MBOA-SIG) requested a waiver of FCC rules that require gating/hopping to be turned off during average power compliance measurements [6]. This group argues that UWB test procedures were developed specifically for pulse-based systems, putting them at an unfair disadvantage. MBOA-SIG also argues that the proposed MB-OFDM system, which hops between three bands, causes no greater interference to licensed services than pulsed UWB devices. Opponents argue that granting the waiver will put MB-OFDM at an unfair advantage as compared to other UWB systems and increase its interference to legacy receivers. To help resolve regulatory questions associated with non-continuous interference, gated Gaussian noise is included in this interference study. This signal eliminates the complexities associated with actual UWB modulations and provides a simple, parameterized theoretical basis for understanding the susceptibility characteristics.

## **1.2. Organization of This Report**

This first report describes the methodology, test system, and procedures developed to characterize UWB emissions and measure susceptibility of C-band satellite DTV receivers. It is divided into five sections in the main body and eight appendices. The main body of this report is a comprehensive, high-level discussion providing orientation and motivation for the reader. Section 2 gives technical descriptions of the interference signals considered as well as discussion on related signal simulation and generation techniques. Section 3 examines interference signal characterization measurements and describes relevant metrics, test and measurement equipment, and procedures. Section 4 discusses technical aspects of the victim receiver. It summarizes relevant communication aspects of DTV systems, simulation of DTV satellite signals, and metrics to assess signal quality degradation. Section 5 describes a test to assess interference susceptibility of satellite DTV receivers to UWB signals.

Appendices to this report contain information supporting the main body. Appendix A describes the mathematics behind simulation of the interference signals. Appendices B and C discuss the operation and specific technical aspects of the vector signal generator used to generate the interference signals. Appendix D explains an efficient means for estimating the amplitude probability distribution of a complex-baseband signal. Appendix E discusses important issues related to signal characterization measurements using the vector signal analyzer. Appendix F provides detailed test system calibration measurements. Appendix G gives hardware specifications. Finally, Appendix H is a glossary of acronyms and units used in this report.

## 2. INTERFERENCE SIGNALS

This study evaluates DS-UWB, Dithered-Pulse Ultrawideband (DP-UWB), MB-OFDM, and gated Gaussian noise signals. DS-UWB and MB-OFDM prototypes existed during the evaluation period; however, since the prototype equipment was constrained by either availability or functionality, we chose to develop our own methods for generating these signals. As shown in Figure 1, these methods required three principal tasks: signal description, computer simulation, and vector signal generation. This section summarizes our approach towards these tasks and associated challenges.

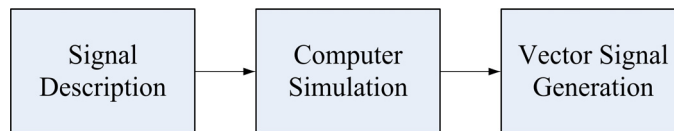


Figure 1. Signal generation tasks.

### 2.1. Signal Description

This subsection provides brief descriptions and signal parameters of the interfering signals evaluated in this study; more detailed mathematical descriptions are provided in Appendix A.

#### 2.1.1. Direct-Sequence Ultrawideband

DS-UWB is currently being considered as an IEEE 802.15 standard [7]. DS-UWB transmits signals in two bands which occupy spectrum approximately from 3.1 to 4.8 GHz and 6.2 to 9.7 GHz. Our interest is chiefly in the lower band which overlays the C-band satellite spectrum.

DS-UWB devices transmit band-limited pulses in two operational modes – sparse mode and DS mode; both modes are illustrated in Figure 2. Binary data modulates codewords composed of 1, 3, 6, 12, or 24 chips. A codeword with length 1 is the trivial case where chip and codeword are equivalent. Lengths 3, 6, and 12 use sparse codes where all but one chip have zero values. Lengths 12 and 24 have a small set of direct-sequence codewords, composed of chips with values of 1, -1, and 0.

Chips are generated at a nominal rate of 1320 million chips per second in the lower band. Slight variations of chip rate are used with length 12 and 24 direct sequence codewords to differentiate transmitters operating in co-located networks. Each codeword conveys 1 bit of information. Hence, shorter codewords have higher data rates. The data rate is reduced by the use of convolution codes with rates 1/2 and 3/4. As an example, a link using a 6 chip sparse codeword and 1/2 rate convolutional code can achieve 110 million bits per second (Mbps).

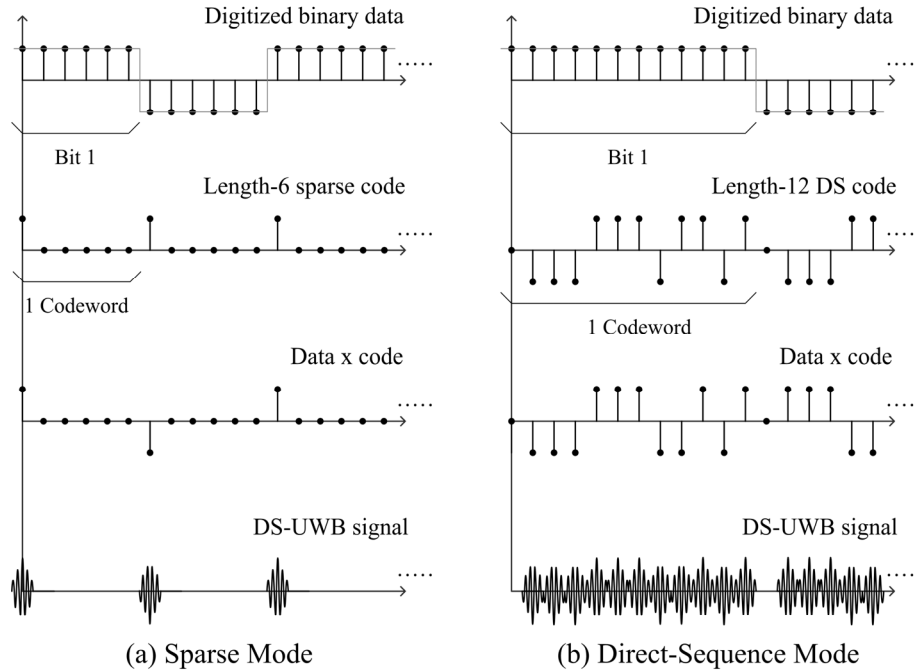


Figure 2. DS-UWB construction: (a) length-6 sparse codeword (1,0,0,0,0,0), and (b) length-12 DS codeword (0,-1,-1,-1,1,1,1,-1,1,1,-1,1).

A single simulated DS-UWB pulse is shown in Figure 3. The root-raised cosine filter, with a roll-off factor of 0.3, limits the occupied spectrum to 1.716 GHz, which is 30% greater than the chip rate.

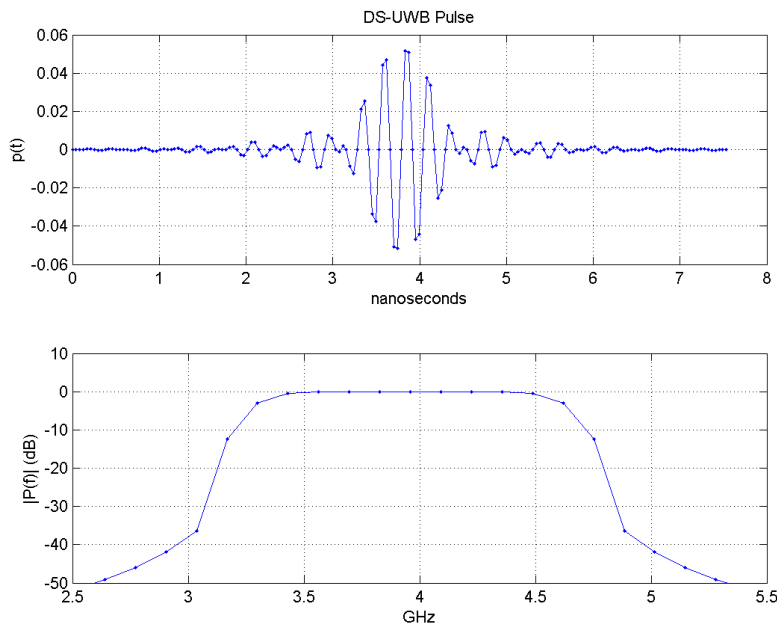


Figure 3. Simulated DS-UWB pulse sampled at 23,760 million samples per second.

Table 1 gives code lengths and codewords for the DS-UWB signals evaluated in this study. The convolutional code rate has no impact on signal characteristics and therefore is not included in the signal parameters that describe the permutations. Shaded rows highlight signals available from prototype equipment supplied by the manufacturer.

Table 1. DS-UWB Signals Considered in This Study

Signal	Code length	Codewords
DS – 1	1	1
DS – 2	3	0,1,0
DS – 3	6	0,0,1,0,0,0
DS – 4	12	0,-1,-1,-1, 1,1,1,-1,1,1,-1,1
DS – 5	12	0,0,0,0,0,0,0,0,1,0,0,0
DS – 6	24	-1,1,-1,-1,1,-1,-1,1,-1,0,-1,0,-1,-1,1,1,1,-1,1,1,1,-1,-1,-1

### 2.1.2. Dithered-Pulse Ultrawideband

DP-UWB is not currently being considered as an IEEE 802.15 standard. However, it is included in our evaluation because it is a conventional pulsed UWB signal.

DP-UWB pulses are position modulated where pulse position is determined by the binary data and a dither factor. The dither factor is the fraction of a symbol period,  $T_{pulse}$ , to which the pulse position is bounded. This factor is often referred to as percentage dither by multiplying it by 100. For example, a 50% dithered pulse carrying a -1 value is bounded from the center of the symbol period to as much as  $T_{pulse}/4$  behind the center. Similarly, the data value 1 positions the pulse ahead of the center of the symbol period by as much as  $T_{pulse}/4$ . Figure 4 depicts pulses that have been position modulated with 50% dithering. Pulse repetition frequencies (PRF) correspond directly to the data rate for binary data. This data rate would be reduced with the likely use of convolutional coding in a practical system.

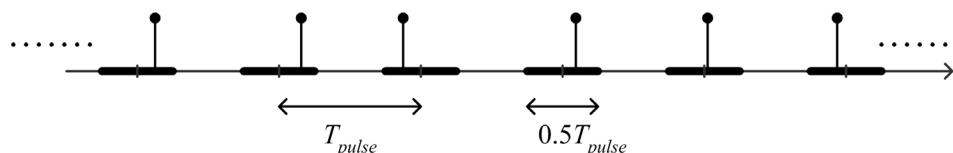


Figure 4. Example of 50% dithered pulses transmitting (...1, 1, -1, 1, 1, -1...).

A single simulated DP-UWB pulse is shown in Figure 5. It is a negative unipolar pulse with an approximate 80-picosecond pulse width measured at a point corresponding to half the maximum pulse amplitude. The DP-UWB pulse frequency response is 10-dB down at 6.3 GHz.

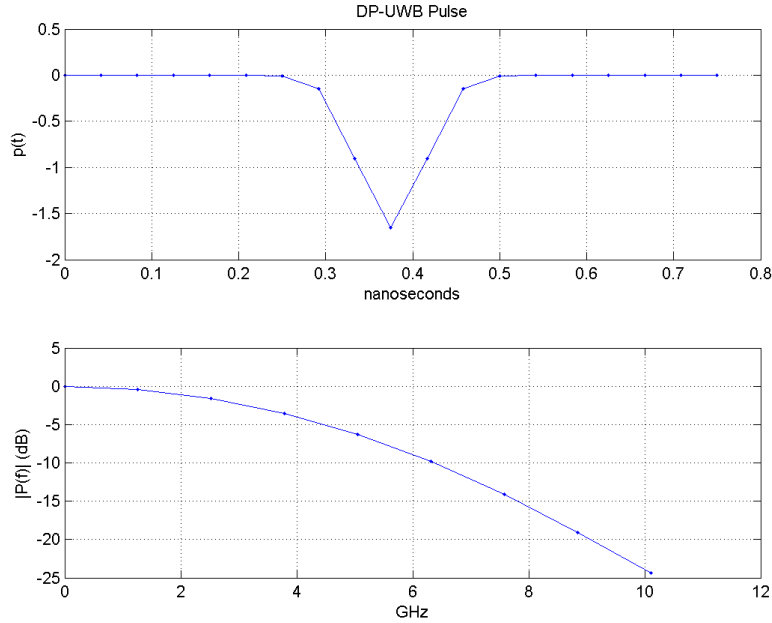


Figure 5. Simulated Gaussian pulse sampled at 24,000 million samples per second.

Table 2 gives PRFs of the DP-UWB signals evaluated in this study. Shaded rows indicate signals that could be generated with a hardware DP generator constructed in lieu of a prototype.

Table 2. 50%-Dithered-Pulse<sup>2</sup> UWB Signals Considered in This Study

Signal	PRF (MHz)
DP – 1	0.1
DP – 2	1
DP – 3	10
DP – 4	100

<sup>2</sup> Negative unipolar pulse with 80-picosecond pulse width.

### 2.1.3. Multi-Band OFDM Ultrawideband

MB-OFDM is currently being considered as an IEEE 802.15 standard [8]. MB-OFDM transmits in any one of fourteen bands whose center frequencies are spaced 528 MHz apart beginning at 3.432 GHz and ending at 10.296 GHz. In this study, we are interested in the band centered at 3960 MHz, which overlaps the C-band satellite spectrum.

A time-frequency code, used to minimize interference between collocated networks, determines the order and number of bands the transmitter hops to and the number of symbol periods the transmitter dwells in a band. For example, a 3/2 time-frequency code would hop over 3 bands and dwell at each band for 2 MB-OFDM symbol periods.

An MB-OFDM symbol consists of a 32-sample zero prefix, a 128-sample data block, and a 5-sample guard interval. These 165 samples, generated at a sampling frequency of 528 MHz, last 312.5 nanoseconds. An example of a single simulated MB-OFDM symbol is depicted in Figure 6. Each MB-OFDM symbol conveys 100 QPSK symbols corresponding to 200 information bits. This throughput is reduced by the convolutional code rates 1/3, 11/32, 5/8, and 3/4. Redundant transmission of data on another frequency band for diversity purposes reduces the data rate further. A 110 Mbps rate corresponds to an 11/32 code rate with 2-band frequency diversity.

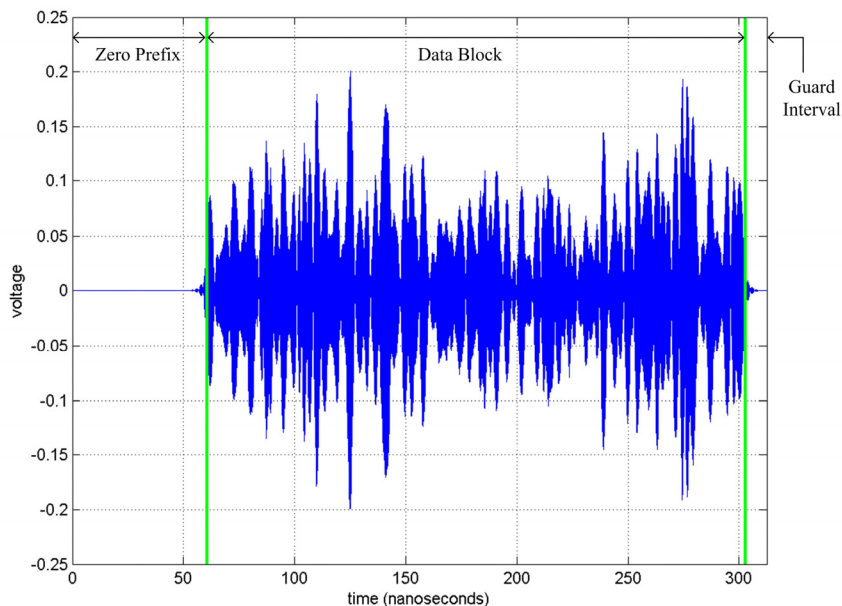


Figure 6. Simulated MB-OFDM symbol with 32-sample zero prefix, 128-sample data block, and 5-sample guard interval.

The 128-sample data block is created by inverse Fourier transforming the coefficients of 128 tones spaced 4.125 MHz apart. The tones include 100 QPSK-modulated data tones, 12 BPSK-modulated pilot tones evenly spaced throughout the data tones, one zeroed tone at the center frequency, 10 BPSK-modulated guard tones near the band edges, and five zero guard tones located at the band edges (which do not add to the bandwidth of the signal). Figure 7 illustrates the tone positions.

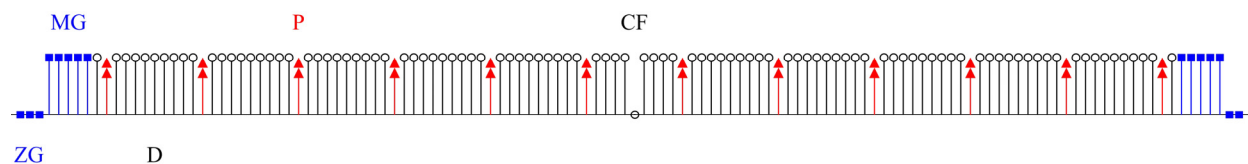


Figure 7. Position of zero guard tones (ZG), modulated guard tones (MG), pilot tones (P), zero center frequency tone (CF), and data tones (D).

Table 3 gives the number of bands and dwells for MB-OFDM signals considered in this study. Shaded rows indicate signals available from the prototype supplied by the manufacturer.

Table 3. MB-OFDM Signals Considered in This Study

Signal	Bands	Dwell
MB – 1	1	1
MB – 2	3	1
MB – 3	3	2
MB – 4	7	1
MB – 5	7	2
MB – 6	7	6
MB – 7	13	1
MB – 8	13	2
MB – 9	13	12

#### 2.1.4. Gated Gaussian Noise

Gaussian noise is a fundamental random process present in all communication systems. It has been studied extensively and provides a good reference to compare other forms of interference. In this study, we investigated how DS-UWB statistics compare with Gaussian noise statistics.

Gating is sometimes used in communication devices to increase signal power beyond the average power limits specified by the FCC. Given integration times that are large compared to a gating period, signal power can be amplified by the reciprocal of the duty cycle while maintaining the same average power. For example, if continuous Gaussian noise is gated with a 25% duty cycle and amplified by 6 dB, it has the same average power as the original continuous signal.

Frequency hopping of an MB-OFDM signal appears as gating to a fixed-frequency narrowband receiver. To help resolve compliance measurement issues for gated/hopped signals related to [6], gated Gaussian noise is considered as a general interference signal with ultra-wide bandwidth and without the complexities associated with actual UWB modulations. Table 4 gives on-times and duty cycles of periodically gated Gaussian noise signals considered in this study.

Table 4. Periodically Gated Gaussian Noise Signals Considered in This Study

GN-01 = Gaussian noise		Duty cycle (percentage of time noise is gated on)			
		50	25	12.5	6.25
On-time (nanoseconds)	10	GN-02	GN-03	GN-04	GN-05
	100	GN-06	GN-07	GN-08	GN-09
	1,000	GN-10	GN-11	GN-12	GN-13
	10,000	GN-14	GN-15	GN-16	GN-17

Table 5 gives the number of bands and dwells for gated-noise signals that emulate the MB-OFDM signals in Table 3. Two distinct gating processes are used for the insertion of prefix and guard intervals and for the frequency hopping due to the time-frequency codes. Both gating processes contribute to the percentage of time that noise is actually on. All gated-noise permutations in Tables 4 and 5 could be generated with a noise diode, an amplifier, and an electronic switch with a fast rise time.

Table 5. Gated Gaussian Noise Signals Emulating MB-OFDM Signals in Table 3

Signal	Bands	Dwells	Percentage of time noise is actually on
GN(MB) – 1	1	1	77.6
GN(MB) – 2	3	1	25.9
GN(MB) – 3	3	2	25.9
GN(MB) – 4	7	1	11.1
GN(MB) – 5	7	2	11.1
GN(MB) – 6	7	6	11.1
GN(MB) – 7	13	1	6.0
GN(MB) – 8	13	2	6.0
GN(MB) – 9	13	12	6.0

## 2.2. Computer Simulation

Computer simulation translates the mathematical description of the signal to samples needed by the vector signal generator. Simulation of realistic, wide-bandwidth signals places a considerable burden on most computers with finite memory and processor resources. Consequently, steps were taken to reduce the complexity of the wireless network system and the number of samples needed to accurately represent the signal produced by it. Although a prototype UWB receiver will not be able to demodulate the simplified signal, from the perspective of the victim receiver, it is indistinguishable from a signal generated by a prototype UWB transmitter. This subsection describes the software implementation of the interference signals at a high level; specific details and further explanation of the computer simulation will be provided in a separate document.

### 2.2.1. Reduction of System Complexity

The operational standards for WPAN systems are still under development [7, 8], but the language and structure will be similar to wireless local area networks (WLAN) as described in the *IEEE 802.11 Handbook* [9]. As depicted in Figure 8(a), wireless network systems are structured into two layers: medium access control (MAC) and physical (PHY). Briefly, the MAC layer supplies a reliable delivery mechanism for data transfer over noisy, unreliable wireless media. It reduces interference between systems by dictating when transmissions occur and how long they last. The PHY layer transmits and receives data over a shared wireless media; it is the interface between the MAC and wireless media. The PHY layer is divided into two sublayers:

physical layer convergence procedure/protocol (PLCP) and physical medium dependent (PMD). The PLCP sublayer provides information needed by the receiver to demodulate the signal. The PMD establishes the mechanism for converting information bits into transmitted signals and from received signals.

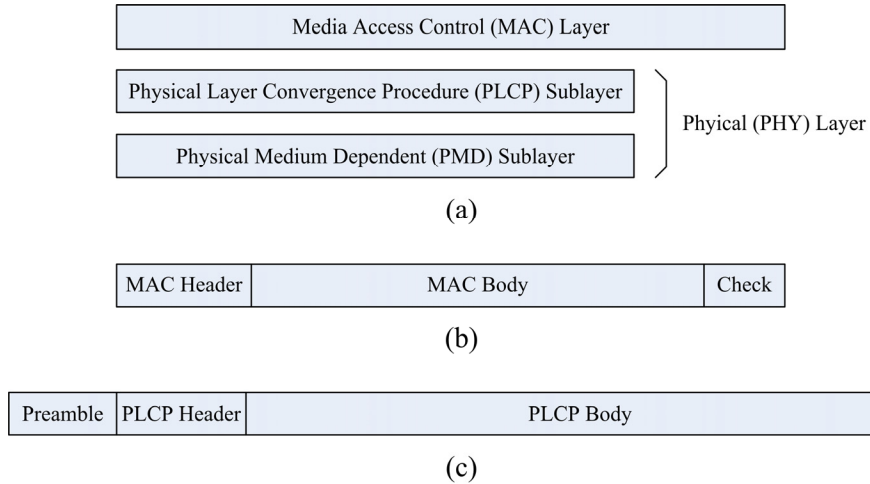


Figure 8. (a) Wireless network layers, (b) MAC frame, (c) PLCP frame.

MAC and PLCP information is organized into frames as shown in Figures 8(b) and 8(c). The MAC frame includes a header, body, and a check sequence. The PLCP frame includes a preamble, header, and body; the PLCP body holds the MAC frame. Figure 9 depicts components of a typical wireless network transmitter where bits representing the PLCP frame are converted to signals for transmission under the control of the PMD sublayer.

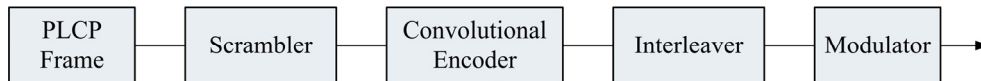


Figure 9. Transmitter PMD components.

Levels of simulation complexity are depicted in Figure 10. The most sophisticated simulation includes MAC control of the PLCP frames. A less complex simulation transmits a steady stream of PLCP frames. The simplest simulation transmits a steady stream of scrambled MAC frames.

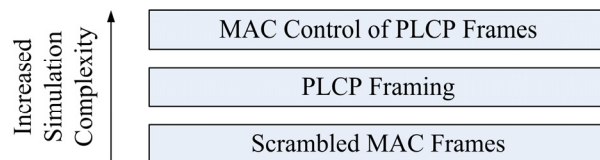


Figure 10. Levels of wireless network simulation complexity.

For the present scope of this study, simulation at the simplest level is adequate. As shown in Figure 11, random data representing the scrambled, convolutionally encoded, and interleaved MAC frame modulates the UWB signals described in Section 2.1 and Appendix A. Justification for this approach is two-fold. First, the MAC frame is the most significant part of the PLCP frame. Second, MAC control of PLCP frames must include consideration of various traffic models, which would detract from questions related to the specific UWB modulators.

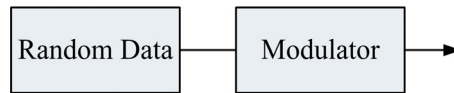


Figure 11. Simplified wireless network simulation. Figures A-1, A-2, and A-3 in Appendix A give specific details of DS-UWB, DP-UWB, and MB-OFDM modulators.

### 2.2.2. Reduction of Samples

For practical purposes, the number of samples and the corresponding sample rate need to be reduced so that reasonably long signal durations can be processed in a timely manner. For example, the sampling rate is often set to 4 or more times the highest frequency of interest. For real signals considered in this study, the highest frequency of interest exceeds 4 GHz, which requires more than 16 GSps. This produces far too many samples to process in a reasonable time for most computers.

Sample rates of signals can be reduced by bandpass filtering the real signal and converting the real-bandpass signal to complex-baseband (CBB) as depicted in Figure 12. Conversion to CBB allows for the use of a sample rate that depends on the bandwidth,  $B$ , of the filter rather than highest frequency of the original signal. Simulation in CBB also has the benefit of generating waveforms readily implemented on the vector signal generator (VSG).

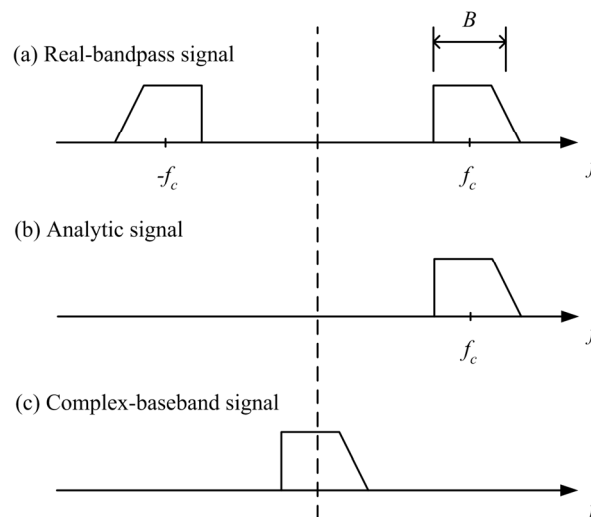


Figure 12. Spectrum amplitude of (a) real-bandpass, (b) analytic, and (c) CBB signals.

### 2.3. Implementation on the Vector Signal Generator

Simulated CBB interference waveforms were implemented on the VSG. A brief description of the VSG is given here with a more detailed description given in Appendix B. Figure 13 shows a highly simplified block diagram of the VSG. The simulated discrete-time CBB signal, stored in fixed-point format as a waveform file, is loaded into VSG memory. The VSG converts the digital in-phase (I) and quadrature-phase (Q) signals to I and Q analog signals using interpolation, digital-to-analog conversion, and analog reconstruction filtering. The analog I and Q signals are the inputs to the I/Q modulator, which converts the CBB signal to a real signal at the RF center frequency determined by the local oscillator (LO).

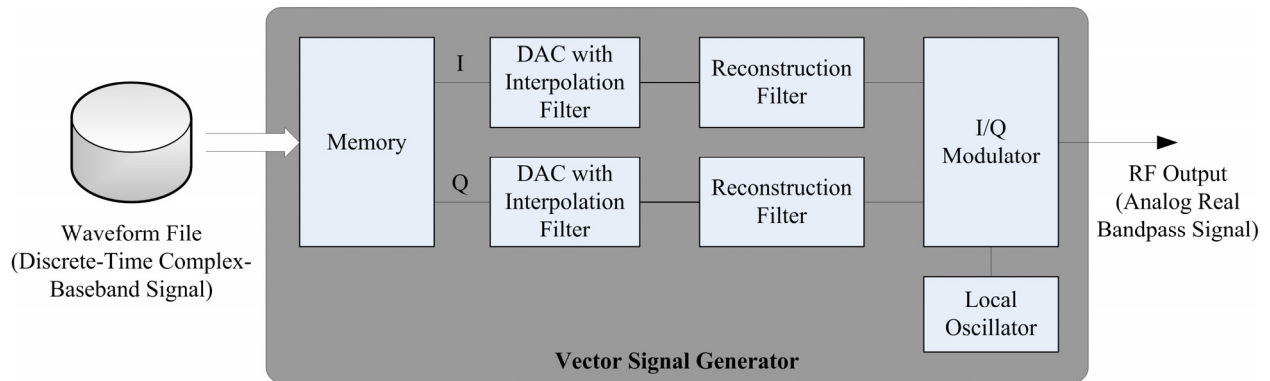


Figure 13. Vector signal generator block diagram. DAC stands for digital-to-analog converter.

The VSG produces an RF output that is somewhat degraded. Imperfect digital-to-analog conversion distorts the desired signal. This distortion is most severe at the band edges. Additionally, LO feed-through, intermodulation products, and other spurious responses from imperfect I/Q modulation can corrupt the desired signal. Appendix B discusses techniques to minimize the amplitude of these undesirable signals. Appendix C provides a detailed discussion of the most prominent VSG impairment, LO feed-through, and describes an experiment that demonstrates that LO feed-through is not a problem for the DTV interference susceptibility test.

### 3. INTERFERENCE CHARACTERIZATION MEASUREMENTS

Interference characterization measurements were made with the vector signal analyzer (VSA), spectrum analyzer (SA), digital oscilloscope (DO), and power meter. These measurements were made at C-band on signals directly out of the VSG. Measurements were also performed on prototypes when available. This section describes metrics used to characterize interference, data needed to compute the metrics, instruments used for collecting the data, and specific settings for the instruments.

#### 3.1. Metrics and Data Needed to Compute Them

Interference signals can be characterized by statistics of the random variable representing the time-varying signal voltage. Measurement and statistical processing is made difficult by the high-frequency content of UWB signals. For example, DS-UWB and DP-UWB pulses shown in Figures 3 and 5 require sample rates of 23.76 GSps and 24 GSps, respectively, to obtain adequate resolution. Currently, digitization at these sample rates requires state-of-the-art oscilloscopes. Fortunately, our interest is in the effect of interference on relatively narrowband receivers. Inside a superheterodyne victim receiver, interference is band-limited and downconverted to CBB along with the desired signal. Consequently, it makes sense to measure and statistically analyze the CBB signal, which can be sampled at slower rates.

Statistics of particular interest are peak voltage, root-mean-square (rms) voltage, amplitude probability distribution (*APD*), power spectral density (*PSD*), and other higher-order statistics [10]. *APD* characterizes a random process by displaying the percentages of time that a signal exceeds certain levels, which can be determined by histogramming or sorting the amplitudes. The sorting method for estimating *APDs* is described in Appendix D. *PSD* is a measure of the average power per unit bandwidth as a function of frequency. It can be determined from the Fourier transformed autocorrelation function or from averaged spectrum magnitudes.

#### 3.2. Description of Test and Measurement Equipment

Previous UWB signal characterization studies [2, 3] relied mostly on the spectrum analyzer, power meter, and digital oscilloscope. In addition, this study utilizes the vector signal analyzer to acquire amplitude and phase samples of the CBB signal. These instruments differ in bandwidth, dynamic range, and the type of data they acquire. This subsection describes each instrument and explains tradeoffs associated with each. Measurement parameters are described for acquiring data necessary to compute metrics that characterize interference signals.

##### 3.2.1. Vector Signal Analyzer

The Agilent 89461A VSA provides approximately 36-MHz maximum bandwidth with 50-dB dynamic range in the maximum bandwidth. In Appendix E, dynamic range is defined and measured. Figure 14 shows a simplified block diagram of the VSA. Signals at the RF input are

attenuated to prevent overload and filtered to reject image frequencies. The RF signal is then downconverted to a final intermediate frequency (IF) of approximately 19 MHz. The final IF signal is converted to a digital IF signal by an analog-to-digital converter (ADC) operating at 95 million samples per second (MSps). The digital IF signal is converted to CBB using digital downconversion. The fastest sampling rate of the I and Q signals is 46.08 MHz corresponding to a 21.7-nanosecond sample period and a 36-MHz span. For the VSA, span refers to the bandwidth where amplitude and phase distortion are negligible. Decimation to slower “cardinal” sampling rates, each related by a factor of 1/2, can be used to generate other cardinal spans. For example, cardinal spans of 18, 9, 4.5, 2.25, 1.125, and 0.5625 MHz correspond to decimation factors of 1/2, 1/4, 1/8, 1/16, 1/32, and 1/64.

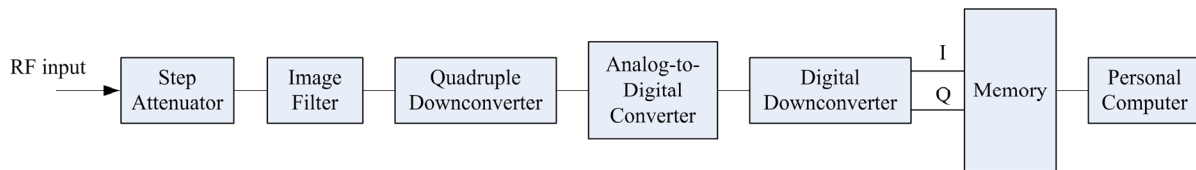


Figure 14. Conceptual block diagram of a vector signal analyzer.

VSA operation is controlled by vendor-supplied software running on a PC. VSA measurement settings include center frequency, span, input range (i.e., maximum signal amplitude), and number of samples. The software commands the VSA to acquire data at the smallest cardinal span greater than the requested span. Data is transferred to the PC and re-sampled to a rate corresponding to the requested span. The re-sampled data can be saved in memory for post-measurement analysis or processed for immediate display. For a more detailed discussion of the VSA refer to *Agilent Application Note 150-15* [11].

The VSA is good for characterizing interference to DTV receivers, since its bandwidth is commensurate to that of the satellite transponder. Furthermore, the VSA provides data with both amplitude and phase. This improves the versatility of the data and reduces the number of measurements required. For example, we are interested in illustrating signal characteristics in a variety of bandwidths corresponding to the satellite transponder, i.e., 36 MHz, the DTV signal used for interference susceptibility tests, i.e., 19.51 MHz, and other legacy systems (to investigate bandwidth scalability of statistics). Rather than remeasure at each bandwidth, digital filters are applied during post processing to achieve the specified processing bandwidths; this would not be possible if only magnitude data were available.

VSA settings for characterizing interference signals are given in Table 6. Settings were chosen with three considerations in mind. First, the maximum VSA bandwidth is used to characterize interference to the satellite DTV channel. Second, it is preferable to use a cardinal span, rather than some arbitrary span, to avoid re-sampling by the vendor supplied software. Finally, at least 100,000 samples, free of correlations introduced by measurement equipment, are necessary to estimate statistics at the 0.01 percentile. Hence, at least  $100,000 \times 36/10 = 360,000$  samples should be measured in the 36-MHz span,  $100,000 \times 4.5/1 = 450,000$  samples should be measured in the 4.5-MHz span, and  $100,000 \times 0.5625/0.1 = 562,500$  samples should be measured in the 0.5625-MHz span.

Table 6. VSA Measurement Settings for Various Post-Processing Bandwidths

Post-Processing Bandwidths (MHz)	Span (MHz)	Number of Samples	Center Frequency (MHz)	Input Range (dBm)
36, 19.51, 10	36	> 360,000	3820	-30
1	4.5	> 450,000		
0.1	0.5625	> 562,500		

Center frequency corresponds to the center of the DTV channel chosen for the interference susceptibility test. An input range of -30 dBm was chosen for these measurements. VSA measurement accuracy is only possible if the range of signal amplitudes resides within the dynamic range of the measurement device. Appendices E and F demonstrate how to set the average power of input signals to ensure accurate VSA measurements.

### 3.2.2. Spectrum Analyzer

The Agilent E4440A spectrum analyzer provides an 8-MHz maximum bandwidth with more dynamic range than the VSA. Figure 15 shows a simplified block diagram of the SA. The signal at the RF input is attenuated and passed through a preselection filter to reject strong out-of-band signals. The sweep generator instructs the SA to sweep over a specified frequency span, which shifts the RF input to a target IF for the two-stage downconverter. The final IF signal is centered at 7.5-MHz and converted to a digital IF signal by the analog-to-digital converter operating at 30 MSps. The digital IF signal is then converted to CBB using a digital downconversion and decimation process. At this point, the complex samples can be processed and displayed, or sent to a PC for post measurement analysis. For our purposes, digital signal processing inside the SA implements traditional swept measurements that involve application of a resolution bandwidth (*RBW*) filter, envelope detector, and video bandwidth (*VBW*) filter; conventional metrics, i.e., peak and root-mean-square (rms) amplitude, are displayed.

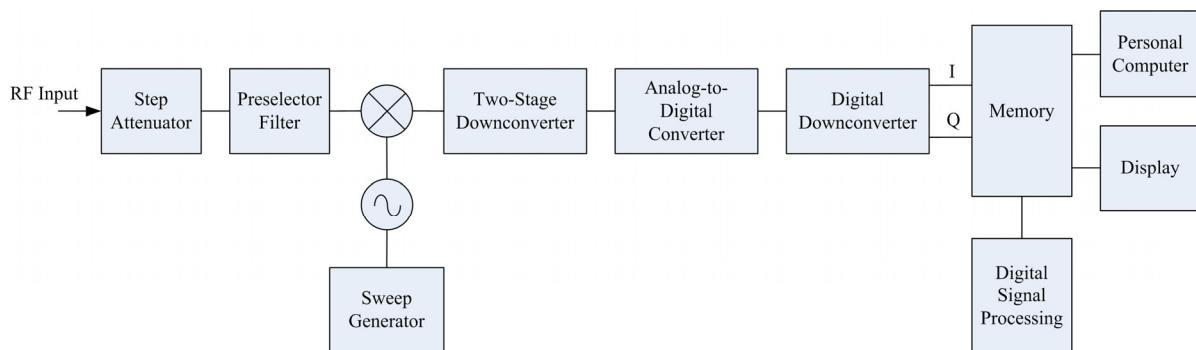


Figure 15. Conceptual block diagram of a digital spectrum analyzer.

SA measurement settings include center frequency, span,  $RBW$ ,  $VBW$ , number of frequency steps ( $N_f$ ), sweep time, and detector type. Center frequency and span define the frequency range the SA sweeps across. The sweep rate and resolution are determined by the span, number of frequency steps, and the length of time allotted for one sweep. For more in-depth discussion of spectrum analyzer operations, the reader is referred to *Agilent Application Note 150* [12].

The maximum SA bandwidth is smaller than that of the satellite DTV channel; however, SA measurements were used to provide  $PSD$  and peak amplitude estimates, verify VSA measurements, perform FCC compliance tests, and monitor signals. Table 7 gives SA settings for characterizing interference signals. Measurements at 3950 MHz are centered on the C-band satellite spectrum. Measurements at 3820 MHz are centered on the DTV channel used for susceptibility testing. Frequency step size, i.e., span divided by the number of frequency steps, is set to one sixth of the  $RBW$  to ensure that spectrum details are not missed.  $VBW$  is much wider than  $RBW$  to ensure peak amplitude accuracy. Sweep time is set to  $1000 \times N_f \times k/RBW$  seconds to ensure rms amplitude accuracy. The Gaussian  $RBW$  filters require  $k = 3$ .

Table 7. Spectrum Analyzer Settings for Characterizing Interference Signals

Center Frequency (MHz)	Span (MHz)	$RBW$ (MHz)	$VBW$ (MHz)	$N_f$	Sweep Time (seconds)	Detector
3950	600	1	50	3600	10.8	Rms, peak
3820	40	0.1		2400	72.0	

### 3.2.3. Digital Oscilloscope

The Tektronix TDS7704B digital oscilloscope DO provides real signal samples with 7-GHz maximum bandwidth and less dynamic range than the VSA and SA. Figure 16 shows a block diagram of the DO. It performs anti-alias filtering and digitizes the signal at a maximum of 20 GSps. Trigger functions allow the user to control when digitization begins. DO measurement settings include sample rate, time scale, voltage scale, and number of samples.

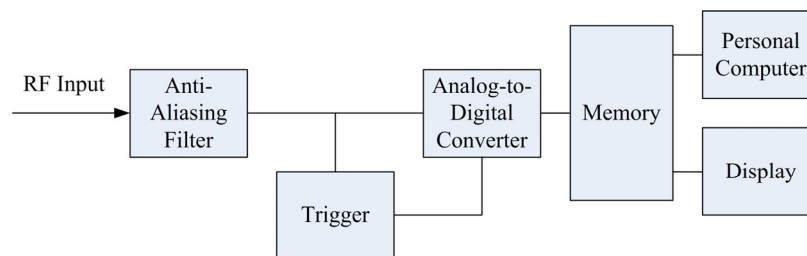


Figure 16. Conceptual block diagram of a digital oscilloscope.

The wide bandwidth of the DO allows for a qualitative “snapshot” of the full-band interference signals to reveal signal parameters such as pulse rise time, signal duration, and gating period.

Table 8 gives typical settings for DO measurements. Actual settings depend on the specific signal characteristics of interest. Maximum sample rate is used to ensure the highest resolution.

Table 8. Digital Oscilloscope Settings for Characterizing Interference Signals

Time Scale (microseconds/div)	Voltage Scale (millivolts/div)	Sample Rate (GSps)
40	50	20
4		

#### 3.2.4. Power Meter

The Agilent 4419B power meter with the 9300A diode average power sensor provides average power measurements with 18-GHz maximum bandwidth and 80-dB dynamic range. Operating in a normal mode, the power meter provides 20 average power measurements per second.

This power meter provides calibrated average power measurements of both RF and IF signals. To get the most accurate reading, it is set to the center frequency of the measured signal and 1024 measurements are averaged; this takes approximately 60 seconds to complete.

## 4. VICTIM RECEIVER

C-band satellite television was chosen as the victim receiver for this interference susceptibility test because C-band receivers operate within the band allocated for UWB emissions, satellite signals are weak and vulnerable to interference, and a number of operational scenarios can be investigated. This section discusses relevant communication aspects of satellite DTV systems, simulation of the DTV satellite signal, and metrics to assess quality; a more general discussion of satellite communication techniques can be found in *Pratt, et al.* [13] and *Couch* [14].

### 4.1. Satellite Digital Television Description

The scope of this study is limited to C-band satellite DTV transmissions that comply with the commonly used Digital Video Broadcast (DVB) recommendations *ETS 300 421* [15] published by the European Telecommunications Standards Institute (ETSI). This subsection discusses the communication aspects of a single transponder channel for satellite DTV systems that comply with DVB recommendations.

#### 4.1.1. MPEG-2 Encoder

DTV video and audio signals are digitized separately, compressed, and then multiplexed into a serial bit stream for transmission. Compression algorithms are applied to minimize the amount of data required to represent the video image or audio, while preserving the level of quality required for the given application. This is achieved by matching spectral characteristics of video and audio signals to the frequency response of human eyes and ears; further compression is achieved by not transmitting static information. DVB uses the MPEG-2 standard for compression.

There are two levels of multiplexing in DVB. At the lowest level, components that make up a program (e.g., video, audio, system-control information) are multiplexed. At a higher level, the programs themselves are multiplexing. The transport subsystem is based on fixed-length packets, each holding 188 bytes of information which represents one MPEG segment. The contents and timing of each packet are identified by packet headers.

#### 4.1.2. Forward Error Correction and Modulation

DVB systems mitigate errors by reducing the baud rate and protecting the signal with forward error correction codes (FEC). Two FEC codes, Reed-Solomon (RS) and convolutional, are used. Briefly, the RS code has a block length of 204 bytes carrying 188 information bytes, or one MPEG segment, and can correct up to 8 byte errors per block. The convolutional code has length 7 and rates that include 1/2, 2/3, 3/4, 5/6, and 7/8. Interleaving (with a depth of 12 bytes) is used to shield the Reed-Solomon decoder from burst errors. FEC-coded bits are mapped into QPSK symbols for transmission. Symbols are band-limited by a root-raised-cosine (RRC) filter with a roll-off factor ( $\alpha$ ) of 0.35 and upconverted to the satellite channel radio frequency (RF).

Table 9 gives  $E_b/N_o$  and signal-to-noise ratio ( $SNR$ ) performance requirements for DVB satellite television.  $E_b/N_o$  is the ratio of energy per bit over noise power spectral density.  $SNR$  requirements are 3 dB higher over  $E_b/N_o$  because QPSK maps two bits into one symbol. If the received signal is above the specified  $E_b/N_o$ , the specified FEC techniques are designed to provide a bit-error rate (BER) between  $10^{-10}$  and  $10^{-11}$  at the output of the RS decoder. This corresponds to less than one uncorrected error “event” per transmission hour. (Although *ETS 300 421* [15] is unclear as to the nature of an error “event,” it is assumed to correspond to an MPEG segment decoding error.)

Table 9. Requirements for One Uncorrected Error “Event” per Transmission Hour [15]

Convolutional Inner Code Rate	$E_b/N_o$ <sup>3</sup> Requirement (dB) for $10^{-11} \leq \text{BER} < 10^{-10}$ After the RS decoder	Corresponding $SNR$ Requirement (dB) for QPSK
1/2	4.5	7.5
2/3	5.0	8.0
3/4	5.5	8.5
5/6	6.0	9.0
7/8	6.4	9.4

<sup>3</sup>  $E_b/N_o$  values include a 0.8-dB modem implementation margin and the 0.36-dB noise bandwidth increase due to the RS code implementation.

#### 4.1.3. Receiver

Figure 17 depicts the two-stage-downconversion superheterodyne architecture typically utilized by satellite DTV receivers. Immediately after the antenna feed, a low-noise block downconverter (LNB) amplifies the received signal and downconverts it to the first IF between 950 and 1450 MHz. The signal is carried to the receiver via coaxial cable, where it is downconverted once more, channel selected, and demodulated. The QPSK demodulator uses RRC filtering to minimize intersymbol interference and maximize  $SNR$ . The demodulated signal is applied to the Viterbi decoder, de-interleaved, and RS decoded. Finally, error-free MPEG segments are demultiplexed, decompressed, and delivered to the television set for viewing. Segments received in error are not passed on. Error concealment is used to hide the effects of their absence.

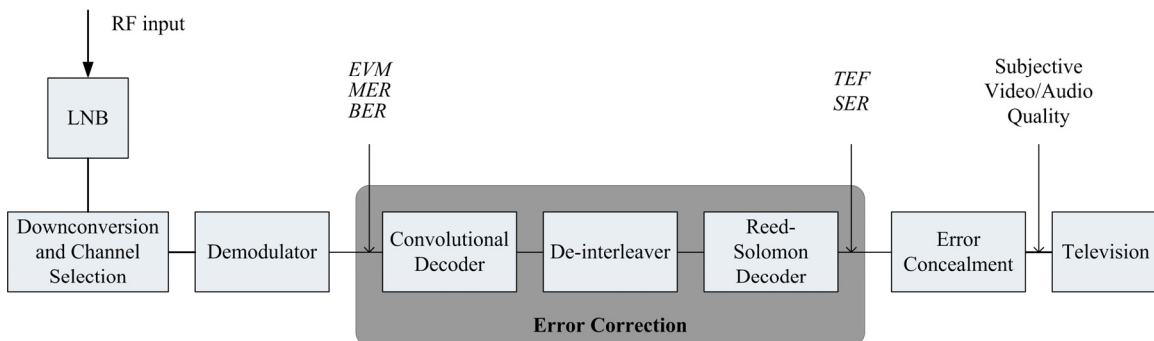


Figure 17. Signal quality metrics measured at different points in a DTV receiver.

## 4.2. DTV Quality Metrics

Video and audio quality is often subjectively evaluated by viewer and listener panels briefly exposed to received images and sounds. Acquisition of subjective quality metrics is qualitative, time consuming, and prone to perceptual error because there are a wide variety of techniques used by receivers to conceal the effects of MPEG segment errors.

Alternatively, quantitative signal quality metrics from various points in the receiver are available from DTV signal monitoring instruments. In this study, signal quality metrics from the Tektronix MTM400 DVB signal monitor are recorded to evaluate degradation of the victim receiver. Available metrics are modulation error rate (*MER*), error vector magnitude (*EVM*), pre-Viterbi bit-error rate (*BER*), and cumulative transport error flag (*TEF*) from which MPEG segment error rate (*SER*) can be computed. Figure 17 shows where the metrics are taken from within the receiver signal processing chain.

*MER* and *EVM* are taken after I/Q demodulation. An example of a demodulated QPSK constellation and its I and Q components are shown in Figure 18.

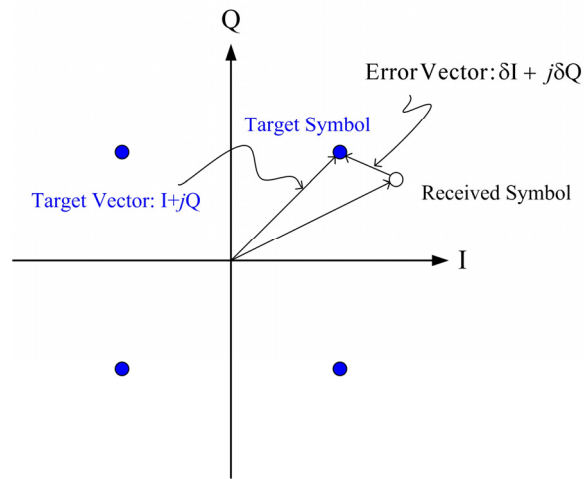


Figure 18. QPSK constellation with both target and received symbols.

Modulation error ratio in dB is defined from these components by

$$MER = 10 \log \left( \frac{\sum_{n=1}^N (I_n^2 + Q_n^2)}{\sum_{n=1}^N (\delta I_n^2 + \delta Q_n^2)} \right),$$

where  $N$  data points are taken to achieve sufficient accuracy. For QPSK, *EVM* can be expressed in terms of *MER* as  $EVM = 10^{2-MER/20}$ .

$SEF$  is post-Reed-Solomon MPEG segment error rate and is calculated from  $TEF$  and Coordinated Universal Time (UTC) as

$$SEF = \frac{TEF(t_2) - TEF(t_1)}{(t_2 - t_1)R_{seg}} ,$$

where  $R_{seg}$  is the MPEG segment rate with units of MPEG segments per second.

### 4.3. Operational Scenario Chosen for DTV Interference Susceptibility Tests

The operational scenario of the victim receiver chosen for this study is shown in Table 10; it corresponds to DTV channel 581 from geostationary satellite Satcom C3 positioned approximately 35,786 km above the equator at 131.0° W longitude. Modulation, compression, and error correction schemes comply with DVB recommendations described in Section 4.1.

Table 10. Satellite Simulation Scenarios for DTV Interference Susceptibility Tests

Transponder Center Frequency	3820 MHz
Modulation	QPSK with root-raised cosine filter ( $\alpha = 0.35$ )
Compression	MPEG-2
Data Rate	26.970353 Mbps
Symbol Rate	$R_S = 19.510468$ Mbaud
Reed-Solomon Error Correction	$R_{RS} = 188/204$
Convolutional Error Correction	$R_{conv} = 3/4, K = 7$
Interleaving	Depth = 12 bytes
Signal-to-Noise Ratio	{8.5, 11.5, 14.5} dB

Calculation of the operational segment rate begins at the byte level. 188 information bytes are packed into a Reed-Solomon codeword, interleaved, and convolutionally encoded. Overhead associated with the error correction scheme is quantified by the rates  $R_{RS} = 188/204$  and  $R_{conv} = 3/4$ . The length in bits of one MPEG segment is

$$\ell_{seg} = \frac{188}{R_{RS} R_{conv}} \times 8 \frac{\text{bits}}{\text{byte}} = 2176 \frac{\text{bits}}{\text{segment}}$$

and the rate at which segments are transmitted is

$$R_{seg} = \frac{m}{\ell_{seg}} R_S ,$$

where  $2^m$  is the modulation alphabet size and  $R_S$  is the symbol rate. For the operational scenario,  $m = 2$  for the QPSK alphabet,  $R_S = 19.51$  Mbaud, and  $R_{seg} = 17,932$  segments per second corresponding to  $T_{seg} = 55.76$  microseconds per segment. The symbol rate and RRC roll-off factor correspond to an occupied bandwidth of approximately  $19.51 \times (1+0.35) = 26.34$  MHz.

*SNR* is determined primarily by the size of the receiving dish, the noise figure of the LNB, and the path length of the signal. Three values, separated by 3 dB, were chosen to include a reasonable set of satellite transmission scenarios; 8.5-dB *SNR* corresponds to the minimum requirement for one uncorrected error event per hour [15].

#### 4.4. Satellite Signal Simulation

Complexity is built into satellite television systems to increase capacity and improve quality of the broadcast. Transponders onboard geostationary satellites capture uplink signals and re-transmit the signals back down to Earth. A typical satellite has twelve 36-MHz transponders. Some satellites double the number of channels by using horizontal and vertical polarizations. The transmitted satellite signal propagates down through the atmosphere and is received by dual-polarized, high-directivity dish antennas.

For the purpose of quantifying interference susceptibility, receiving a “live” satellite signal presents significant disadvantages. Interference can be introduced by the cross-polarized channel on the same frequency, the co-polarized signal on the adjacent channel, and devices located near the receiving antenna. The signal is weakened by attenuation and depolarization effects of the atmosphere. Distortion is caused by nearby ground reflections. Also, “live” video content can be inconsistent and unpredictable. These problems are alleviated by simulating the satellite signal and coupling that signal, along with the simulated interference signal, to the victim receiver with a coaxial cable and a directional coupler rather than a pair of antennas.

Figure 19 shows a block diagram for the satellite signal generator used in this study. The digital video stream is SMPTE-259M, the native video format for MPEG-2, and therefore provides the highest quality input signal. The video clip used is “Flower Garden” from the International Telecommunication Union Recommendation *ITU-R BT.802.1* [16]. This clip is 20 seconds long and repeats itself forward and then backward to minimize discontinuity. The steady scan and detailed video content of “Flower Garden” provides a scene with lots of spatial and temporal information that constantly forces the encoder to generate new digital video. The encoder creates a 26.97-Mbps MPEG-2 bit stream, the modulator adds FEC and creates a 19.51-Mbaud QPSK-modulated signal centered at 70 MHz, and two upconversion stages shift the signal to 3820 MHz. Details on the upconverter are provided in Appendix F.

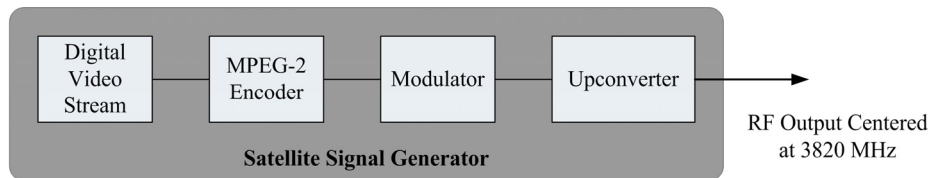


Figure 19. Block diagram for the satellite signal generator. Hardware specifications are in Appendix G.

## 5. INTERFERENCE SUSCEPTIBILITY TESTS

This section provides technical details and justification for tests to assess ultrawideband interference susceptibility of C-band satellite DTV receivers.

### 5.1. Methodology

DVB error correction and concealment schemes cause steep receiver performance curves where a 1-dB difference in *SNR* can cause abrupt changes in picture quality. For our operational scenario, the received picture is seemingly perfect at an *SNR* of 6 dB, yet totally blanked by errors at 4 dB. To resolve this abrupt change in performance, the test system and procedure were designed for precision and repeatability.

The developed test system:

- simulates interference signals in software, so the widest range of UWB signal parameters are available for testing;
- generates interference signals with a VSG from simulated waveforms, so interference amplitude is precisely controlled;
- characterizes interference signals with a VSA, which provides both signal amplitude and phase information for post-measurement filtering and analyses;
- simulates the satellite signal, so that scene content and *SNR* are controlled;
- conductively couples signals to the satellite receiver, so uncertainties introduced by radio channel interference, attenuation, and distortion are eliminated;
- evaluates performance degradation quantitatively with signal quality metrics from an MPEG stream monitor rather than subjective quality metrics;
- is completely characterized, so that its effects on the test are known.

Also, the test procedure:

- is under software control to eliminate procedural errors;
- calibrates the measurement system at the beginning of each test to ensure consistency and system integrity.

### 5.2. Test System

A block diagram of the measurement system is shown in Figure 20. Characterization measurements and component specifications are provided in Appendices F and G. The system is comprised of five subsystems: (1) interference signal generation, (2) satellite signal generation, (3) coupling, (4) victim receiver, and (5) calibration.

Interference signals are generated from software simulated waveforms with a VSG. The VSG provides 0.01-dB amplitude control and is capable of completely turning off the interference signal and terminating the port in 50 ohms. Satellite signals are simulated and step variable attenuator VA provides 1-dB control of the satellite *SNR*. A switch was provided that can completely shut the satellite signal off and terminate the port in 50 ohms during calibration.

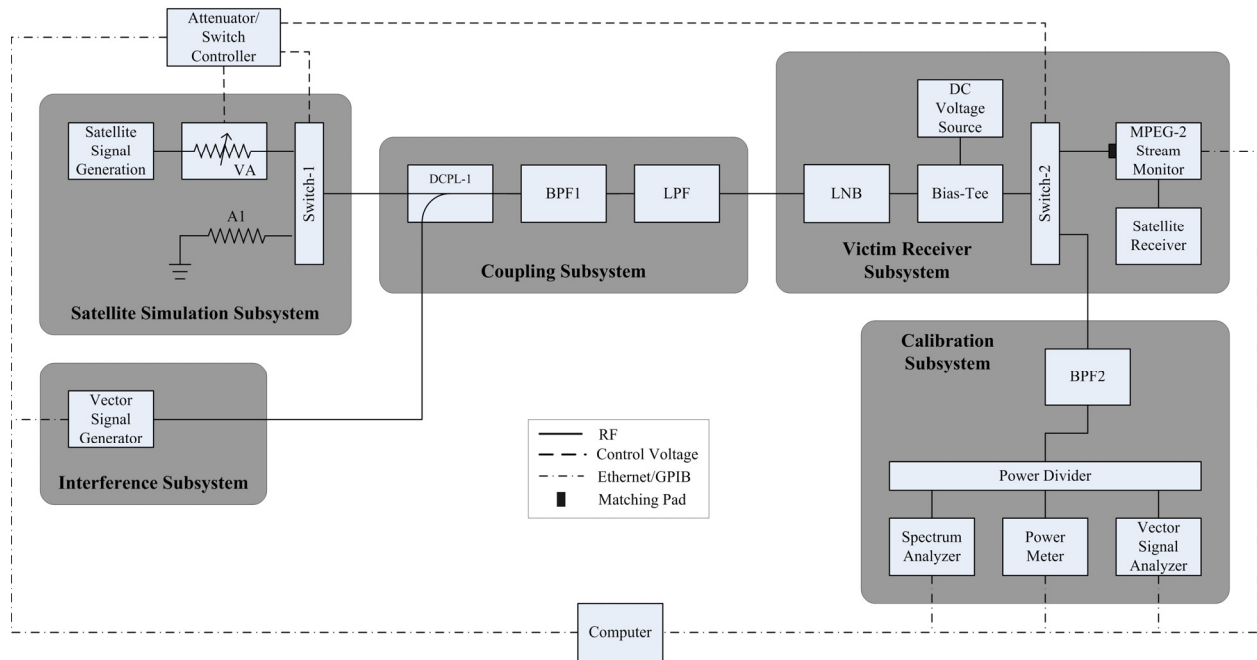


Figure 20. Block diagram for DTV interference susceptibility test. System calibration measurements are in Appendix F. Hardware specifications are in Appendix G.

Satellite and interference signals are added via the coupling subsystem. The interfering signal is applied to the port of directional coupler DCPL-1 that attenuates the signal by 10 dB. The bandwidth of bandpass filter BPF1 corresponds to that of the satellite transponder channel. Lowpass filter LPF assists BPF1 in removing unwanted mixing products introduced by the satellite simulator upconverter. These filters were not included in the satellite simulation subsystem because they also band-limit the interfering signal. Limiting the bandwidth of the interfering signals ensures that performance degradation is due to co-channel interference rather than LNB compression due to out-of-band interference. It also ensures that signals generated by other VSGs or prototype devices will have the same interference bandwidth.

In the receiver subsystem, the LNB downconverts signals to L-band. A bias-tee provides the LNB with the necessary dc voltage and impedance match. The MPEG stream monitor provides a pass-through, L-band signal for the satellite receiver. Scenes transmitted by the satellite simulator can be viewed on a video monitor attached to the satellite receiver. Switch-2 enables the signal to be directed to either the MPEG stream monitor or the calibration subsystem.

In the calibration subsystem, measurements made during each test are performed with the VSA and power meter. The SA is used for signal monitoring and diagnostics. Bandpass filter BPF2 is used to limit the bandwidth of the noise amplified by the LNB and measured by the power meter. BPF2 bandwidth is much wider than that of BPF1 and the VSA, so it does not influence VSA calibration measurements. Care was taken to ensure that VSA measurements are made within the dynamic range of the system and measurement instrument (see Appendix E).

### 5.3. Procedures

A single DTV interference susceptibility test, for any one interference signal given in Section 2.1, involves system calibration followed by quality-metric acquisition.

#### 5.3.1. Calibration

At the beginning of each test, the system is calibrated to ensure that all hardware is operating properly and the satellite signal and interference amplitudes are set properly. The calibration procedure consists of setting the amplitude of the satellite simulator to a level that corresponds to the test *SNR* and the amplitude of the interference signal to a level that affords an accurate VSA measurement. Measurements of the satellite signal plus system noise, interference plus system noise, and system noise alone are then made with the VSA and power meter. These measurements are used in post-measurement processing to precisely determine *SNR* and interference-to-noise ratio (*INR*) conditions present during the test.

#### 5.3.2. DTV Quality Metric Acquisition

DTV quality metrics are acquired with the following procedure at discrete interference levels:

1. Interference is turned off and the receiver is allowed to acquire and demodulate the desired satellite signal in the absence of interference for 20 seconds.
2. Interference at the specified amplitude is applied for approximately 200 seconds.
3. During the time of interference exposure, *MER*, *EVM*, *BER*, *TEF*, and UTC time are sampled at about 3 samples per second and written as a single record to a data file.

During coarse-resolution acquisition, this cycle is repeated at increasing interference amplitudes separated by 2-dB intervals, beginning at an interference level that has negligible effect on signal quality and ending where *SER* is in excess of  $10^{-1}$ . The fine-resolution acquisition begins 2 dB below the interference level where the first *TEF* was counted in the coarse-resolution acquisition. Amplitude is incremented in 0.1-dB steps until  $10^{-1}$  *SER* is once again achieved.

Data from the fine-resolution acquisition is used to determine the “threshold of visibility,” i.e., *SER* where degradation is first perceived. Video quality studies have shown that this threshold correlates to approximately  $SER \approx 10^{-4}$  [17]. From the standpoint of a Bernoulli experiment, where independent interference samples degrade reception of independent MPEG segments, 200 seconds of applied interference is adequate for estimating the *SER*.

## 6. SUMMARY

This report gives procedures for statistical characterization of UWB interference signals and assessment of interference susceptibility of C-band satellite television receivers. Our approach is to inject carefully characterized interference into an operating narrowband receiver and measure the susceptibility of the receiver with precisely defined signal quality metrics.

The victim receiver chosen for this interference susceptibility test is C-band satellite digital television. This receiver demodulates signals transmitted in the 3.7 to 4.2 GHz frequency range, which lies within the band allocated for UWB devices. We chose to generate the satellite signal in the laboratory rather than use an unpredictable live signal, to generate interference signals with a vector signal generator rather than rely solely on prototype devices, and to perform signal and system characterization measurements primarily with the vector signal analyzer to provide comprehensive data capable of being post-processed in many ways.

Specifically, interference signals are simulated in software (see Section 2.2 and Appendix A), so the widest range of UWB signal parameters are available for testing, and generated with a VSG (see Section 2.3 and Appendix B), so interference amplitude is precisely controlled.

Characterization of the interference signals with a VSA (see Section 3.2.1) provides both signal amplitude and phase information for post-measurement filtering and analyses. Satellite signal simulation (see Section 4.4) provides control over the scene content and *SNR*. Signals are conductively coupled to the satellite receiver to eliminate uncertainties introduced by radio channel interference, attenuation, and distortion. Signal quality metrics, i.e., *MER*, *EVM*, *BER*, and *SER*, from an MPEG stream monitor (see Section 4.2) are used to evaluate performance degradation quantitatively. Finally, the test procedure is under software control to eliminate procedural errors and calibrates the measurement system at the beginning of each test to ensure consistency and system integrity.

Comprehensive data acquired will be analyzed to determine if there are common signal characteristics that predict interference potential. Results will be useful for regulatory agencies that are currently charged with defining UWB emission limits and corresponding compliance measurement procedures. Results will also be useful to the communications industry that will only thrive if compliance measurement procedures fairly evaluate interference potential of all UWB signals.

## 7. ACKNOWLEDGMENTS

The authors recognize John McCorkle of Freescale, Inc. for his leadership, insight, and insistence on the highest quality. We learned a great deal from working with John in all relevant technical areas. Dr. Paul Runkle of Signal Innovations provided a wealth of expertise in the field of digital signal processing. Given that signal processing was the crux of this project, Paul made significant contributions by ensuring the integrity and efficient execution of our simulations.

This investigation required a number of ITS engineers with a broad range of expertise, some of whom are not included in the list of authors. The authors recognize J. Randy Hoffman, Richard Statz, and Steven Engelking for developing much of the low level software routines needed to automate the test; Stephen Wolf for his expertise in video quality assessment; Frank Sanders for sharing knowledge learned in previous interference tests on C-band earth station receivers [18]; Dr. Roger Dalke for his knowledge of random processes and experimental uncertainty analyses, and his critical eye; Andrew Rogers and Michael Mitchell for their attention to detail in hardware construction and signal characterization measurements; and Dr. William Kissick for his support and leadership.

## 8. REFERENCES

- [1] “First Report and Order in the matter of ET Docket 98-153 (Revision of Part 15 of the Commission’s Rules Regarding Ultra-Wideband Transmission Systems),” *FCC 02-48*, adopted Feb. 14, 2002, released Apr. 22, 2002.
- [2] W.A. Kissick, Ed., “The temporal and spectral characteristics of ultrawideband signals,” NTIA Report 01-383, Jan. 2001.
- [3] J.R. Hoffman, M.G. Cotton, R.J. Achatz, R.N. Statz, and R.A. Dalke, “Measurements to determine potential interference to GPS receivers from ultrawideband transmission systems,” NTIA Report 01-384, Feb. 2001.
- [4] J.R. Hoffman, M.G. Cotton, R.J. Achatz, and R.N. Statz, “Addendum to NTIA Report 01-384: Measurements to determine potential interference to GPS receivers from ultrawideband transmission systems,” NTIA Report 01-389, Sep. 2001.
- [5] J.R. Hoffman, E.J. Haakinson, and Y. Lo, “Measurements to determine potential interference to public safety radio receivers from ultrawideband transmission systems,” NTIA Report 03-396, Apr. 2003.
- [6] “Office of Engineering and Technology Declares MBOA-SIG Request for a Waiver of Part 15 for an Ultra-Wideband System to be a “Permit-but-Disclose” Proceedings for Ex Parte Purposes,” *Public Notice, ET Docket No. 04-352, DA 04-2793*, released Sep. 3, 2004.
- [7] R. Kohno, M. Welborn, and M. McLaughlin, “DS-UWB Physical Layer Submission to 802.15 Task Group 3a,” *IEEE P802.15-04/0137r0*, Mar. 2004.
- [8] A. Batra, et al., “Multi-band OFDM Physical Layer Proposal for IEEE 802.15 Task Group 3a,” *IEEE P802.15-03/268r3*, Mar. 2004.
- [9] B. O’Hara and A. Petrick, *IEEE 802.11 Handbook*, New York, NY: IEEE Press, 1999.
- [10] C.L. Nikias and A.P. Petrotulu, *Higher-Order Spectra Analysis*, Upper Saddle River, NJ: PTR Prentice Hall, 1993.
- [11] Agilent, “Vector Signal Analysis Basics,” *Application Note 150-15*.
- [12] Agilent, “Spectrum Analyzer Basics,” *Application Note 150*.
- [13] T. Pratt, C. Bostian, and J. Allnutt, *Satellite Communications*, John Wiley and Sons, 2003.
- [14] L.W. Couch, *Digital and Analog Communication Systems*, New York, NY: Macmillan Publishing Company, 1987.
- [15] ETS 300 421: “Digital broadcasting systems for television, sound, and data services: Framing structure, channel coding, and modulation for 11/12 GHz satellite services,” *European Telecommunications Standards Institute*, Dec. 1994.

- [16] ITU-R BT.802.1, “Test Pictures in Sequences for Subjective Assessments of Digital Codecs Conveying Signals Produced According to Recommendation ITU-R BT.601,” *International Telecommunication Union*, Jul. 1994.
- [17] J.C. Whitaker, “Digital television transmission systems,” Ch. 13 in *Standard Handbook of Video and Television Engineering*, J.C. Whitaker, Ed., New York, NY: McGraw-Hill, 2000.
- [18] F. Sanders, “Measurements of pulsed co-channel interference in a 4-GHz digital earth station receiver,” NTIA Report 02-393, May 2002.
- [19] ETS TR 101 290: “Digital video broadcasting (DVB); Measurement guidelines for DVB systems,” *European Telecommunications Standards Institute*, v1.2.1, 2001.
- [20] J.W. Modestino and B. Sankur, “Modelling and analysis of impulsive noise,” Part VII, Section 6 in *Communication Systems and Random Process Theory*, J.K. Skwirzynski, Ed., Alphen aan den Rijn, The Netherlands: Sijthoff & Noordhoff, 1978.
- [21] Agilent Technologies, Inc., Application Note 57-2, “Noise Figure Measurement Accuracy – The Y-Factor Method,” Mar. 19, 2004.

## APPENDIX A: MATHEMATICAL SIGNAL DESCRIPTION

This section provides mathematical expressions for  $u(t)$ , i.e., the real-valued representation of interference signals pertinent to this study.

### A.1. Direct-Sequence Ultrawideband

A block diagram of the simulated direct-sequence ultrawideband (DS-UWB) transmitter is shown in Figure A-1.

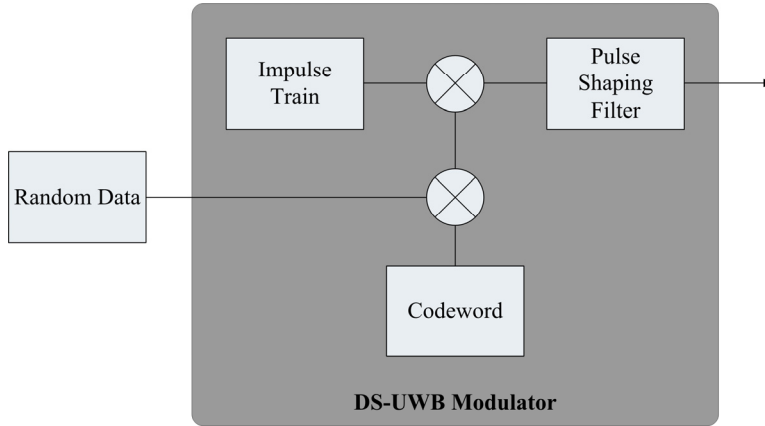


Figure A-1. Simulated DS-UWB transmitter block diagram.

The simulated DS-UWB signal is mathematically described by

$$u(t) = \sum_{k=-\infty}^{\infty} \sum_{l=1}^L d_k c_l p_{DS}(t - kLT_{chip} - (l-1)T_{chip}) ,$$

where  $d_k$  is the  $k^{\text{th}}$  random data element with values  $\{1, -1\}$ ,  $L$  is the codeword length with values of  $\{1, 3, 6, 12, \text{ and } 24\}$ ,  $c_l$  is the  $l^{\text{th}}$  codeword chip with values  $\{1, 0, -1\}$ , and  $T_{chip}$  is the chip period.

The impulse response of the pulse shaping filter is

$$p_{DS}(t) = h_{rrc}(t) \sin(6\pi f_{chip} t) ,$$

where  $h_{rrc}(t)$  is the impulse response of the root-raised-cosine (RRC) filter and  $f_{chip}$  is the chip rate. RRC filters are often specified by their frequency response

$$H_{rrc}(f) = \begin{cases} 1 & |f| \leq f_{co}(1 - \alpha) \\ 0 & |f| > f_{co}(1 + \alpha) \\ \sqrt{\frac{1 + \cos[\pi(|f| - f_{co}(1 - \alpha))/2\alpha f_{co}]}{2}} & f_{co}(1 - \alpha) < |f| \leq f_{co}(1 + \alpha) \end{cases}$$

where  $f_{co}$  is the filter cutoff frequency equal to  $f_{chip}/2$  and  $\alpha$  is the roll-off factor.

## A.2. Dithered-Pulse Ultrawideband

A block diagram of the simulated dithered-pulse ultrawideband (DP-UWB) transmitter is shown in Figure A-2.

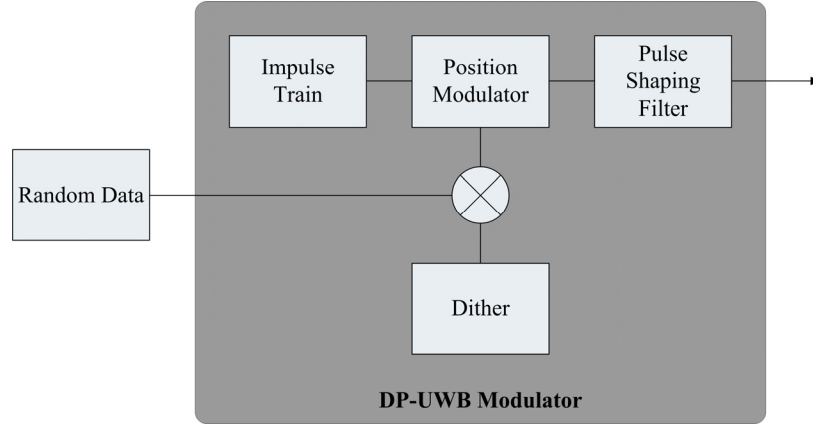


Figure A-2. Simulated DP-UWB block diagram.

The simulated DP-UWB signal is mathematically described by

$$u(t) = \sum_{k=-\infty}^{\infty} p_{DP} \left( t - kT_{pulse} + \frac{T_{pulse}}{2} + \frac{d_k \beta_k T_{pulse}}{2} \right),$$

where  $p_{DP}$  is the pulse-shaping filter impulse response,  $T_{pulse}$  is the average pulse repetition period, and  $d_k$  is the  $k^{\text{th}}$  random data element with values  $\{1, -1\}$ .  $\beta_k$  is the  $k^{\text{th}}$  dithered position relative to  $T_{pulse}$ , which is uniformly distributed with a probability density

$$q(\beta) = \begin{cases} 1/\beta_{max} & 0 < \beta < \beta_{max} \\ 0 & \text{otherwise} \end{cases},$$

where  $\beta_{max}$  is the dither fraction, which is a constant bounded by  $0 < \beta_{max} \leq 1$ .

The pulse-shaping filter has a Gaussian frequency response

$$P_{DP}(f) = \exp(-\sigma^2 f^2) ,$$

where

$$\sigma = \sqrt{\frac{\ln 2}{2B^2}}$$

and  $B$  is the 3-dB bandwidth.

### A.3. Multi-Band OFDM Ultrawideband

A block diagram of the simulated multi-band OFDM (MB-OFDM) transmitter is shown in Figure A-3.

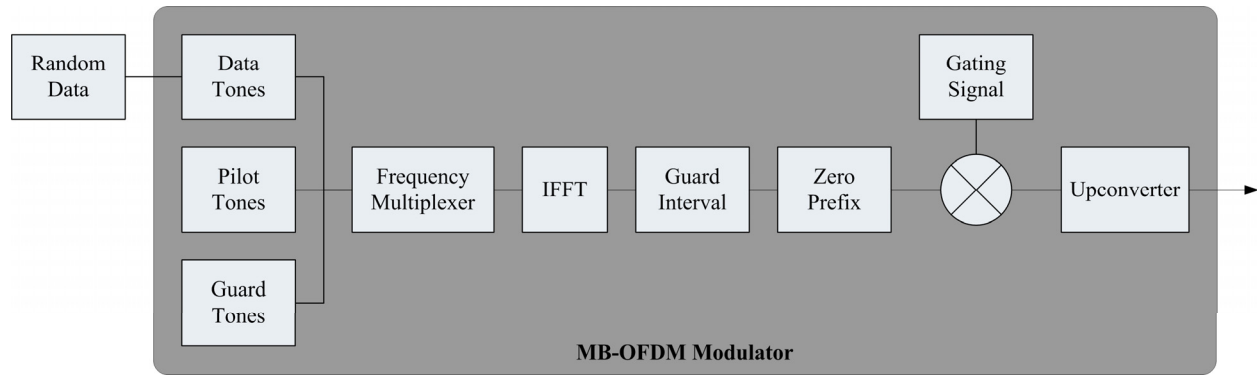


Figure A-3. Simulated MB-OFDM transmitter block diagram.

Mathematical description of the MB-OFDM signal begins with defining the 128-tone coefficient vector

$$D_n = \begin{cases} 0 & n = \{1\} & \text{center} \\ 0 & n = \{63, 64\}, \{65, 66, 67\} & \text{zero guard} \\ \exp\left(j\pi\left(a_n + \frac{1}{4}\right)\right) & n = \{58, 59, 60, 61, 62\}, \{68, 69, 70, 71, 72\} & \text{modulated guard} \\ \exp\left(j\pi\left(a_n + \frac{1}{4}\right)\right) & n = \{6, 16, 26, 36, 46, 56\}, \{74, 84, 94, 104, 114, 124\} & \text{pilot} \\ \exp\left(j\pi\left(\frac{a_n}{2} + \frac{1}{4}\right)\right) & \text{otherwise} & \text{data} \end{cases}$$

where  $a_n$  is the  $n^{\text{th}}$  coefficient value that modulates data, pilot, and modulated guard tones. These coefficients take on values of  $\{0, 1, 2, 3\}$ ,  $\{0, 1\}$ , and  $\{0, 1\}$  for data, pilot, and modulated guard tones respectively. Indices for the tone coefficient vector can be translated to actual frequencies by the equation

$$f = \begin{cases} f_c + (n-1)\Delta f & 1 \leq n \leq 64 \\ f_c + (n-129)\Delta f & 65 \leq n \leq 128 \end{cases} ,$$

where  $f_c$  is the center frequency and  $\Delta f$  is the 4.125-MHz tone spacing.

Random coefficients QPSK modulate the data tones. A fixed pattern of coefficients  $\{0, 1, 0, 0, 1, 0, 0, 1, 0, 0, 1, 0\}$  randomized by a bit from a 127-bit pseudorandom sequence, BPSK modulates the pilot tones. The same 127-bit pseudorandom sequence BPSK modulates the modulated guard tones between symbols. Guard tones within the same symbol are differentiated by a distinct offset into the 127-bit pseudorandom sequence.

The tone coefficients are inverse Fourier transformed to data block samples by

$$d_m = \frac{1}{N} \sum_{n=0}^{N-1} D_n \exp\left(\frac{j2\pi mn}{N}\right) \quad m = 0, 1, 2, \dots, N-1 ,$$

where  $D_n$  is the  $n^{\text{th}}$  QPSK symbol and  $N = 128$ . The MB-OFDM symbol (see Figure 6) is formed by placing the data block between the 32-sample zero prefix and 5-sample guard interval suffix making the total symbol length,  $L$ , 165 samples in duration. The  $k^{\text{th}}$  MB-OFDM symbol is

$$u_{k,l} = \begin{cases} 0 & 0 < l \leq 32 \\ d_{l-33} & 32 < l \leq 160 \\ 0 & 160 < l \leq 165 \end{cases} .$$

The simulated MB-OFDM signal is mathematically described as

$$u(t) = \Re\left(\left(\sum_{k=-\infty}^{\infty} \sum_{l=1}^L u_{k,l} h_{\text{rect}}(t - kT_{\text{OFDM}} - (l-1)\Delta t)\right) \exp(-j2\pi f_c t)\right) ,$$

where  $h_{\text{rect}}$  is a filter with a rectangular frequency response bounded by  $\pm 1/(2\Delta t)$ ,  $T_{\text{OFDM}} = L\Delta t = 312.5$  nanoseconds is the MB-OFDM symbol period,  $\Delta t = 1/(N\Delta f) \approx 1.9$  nanoseconds, and  $\Re$  denotes the real part of a complex number.

Finally, MB-OFDM signals hop between 14 band center frequencies according to the specified time-frequency code. The effect the time-frequency code has on a single frequency is simulated by multiplying the signal by the gate function  $g(t; T = bT_{\text{OFDM}}, \tau = dT_{\text{OFDM}})$ , where  $b$  is the number of bands,  $d$  is the number of periods the signal dwells in each band. The periodic gating function shown in Figure A-4 is defined mathematically as

$$g(t; T, \tau) = \sum_{k=-\infty}^{\infty} R(t - kT; \tau) \quad \text{where} \quad R(t; \tau) = \begin{cases} 1 & 0 \leq t < \tau \\ 0 & \text{otherwise} \end{cases} \quad \text{and} \quad T > \tau .$$

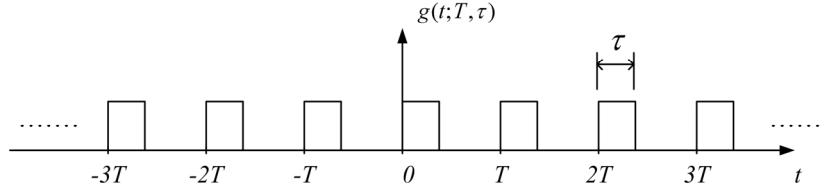


Figure A-4. Periodic gating function.

#### A.4. Gated Gaussian Noise

A block diagram of the simulated gated Gaussian-noise source is shown in Figure A-5.

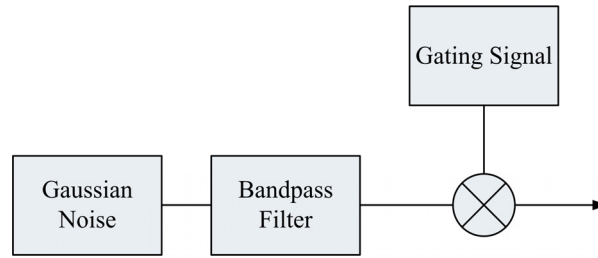


Figure A-5. Simulated gated Gaussian noise transmitter block diagram.

Gated Gaussian noise is described by

$$u(t; T, \tau) = (n(t) * h_{BPF}(t))g(t; T, \tau) ,$$

where  $*$  is the convolutional operator and  $n(t)$  is a zero-mean Gaussian random process with the probability density

$$q(n) = \frac{1}{\sqrt{2\pi}\sigma_n} \exp\left(\frac{-n^2}{2\sigma_n^2}\right) ,$$

where  $\sigma_n$  is the standard deviation of  $n(t)$ .

## APPENDIX B: VECTOR SIGNAL GENERATOR OPERATION

The dual arbitrary waveform generator (AWG) inside the Agilent E8267C Vector Signal Generator (VSG) is used in this study to generate various types of interference signals. Complex-baseband (CBB) waveforms are simulated in software, loaded into VSG memory, and generated by the dual AWG. This appendix describes instrument operation, techniques to optimize RF performance, relevance of these techniques to our study, conditioning of simulated waveforms, and VSG operating procedures.

### B.1. Operation in the Dual AWG Mode

A block diagram of the VSG operating in the dual AWG mode is shown in Figure B-1. Digital in-phase (I) and quadrature-phase (Q) signals, previously loaded into memory, are converted to analog I and Q signals by digital-to-analog converters (DACs) with digital interpolation filters and analog reconstruction (lowpass) filters. Interpolating filters increase the data rate by a factor of four and ease requirements of the reconstruction filters. Reconstruction filters smooth the stair-step responses that are present in the analog I and Q signals at the output of the DACs.

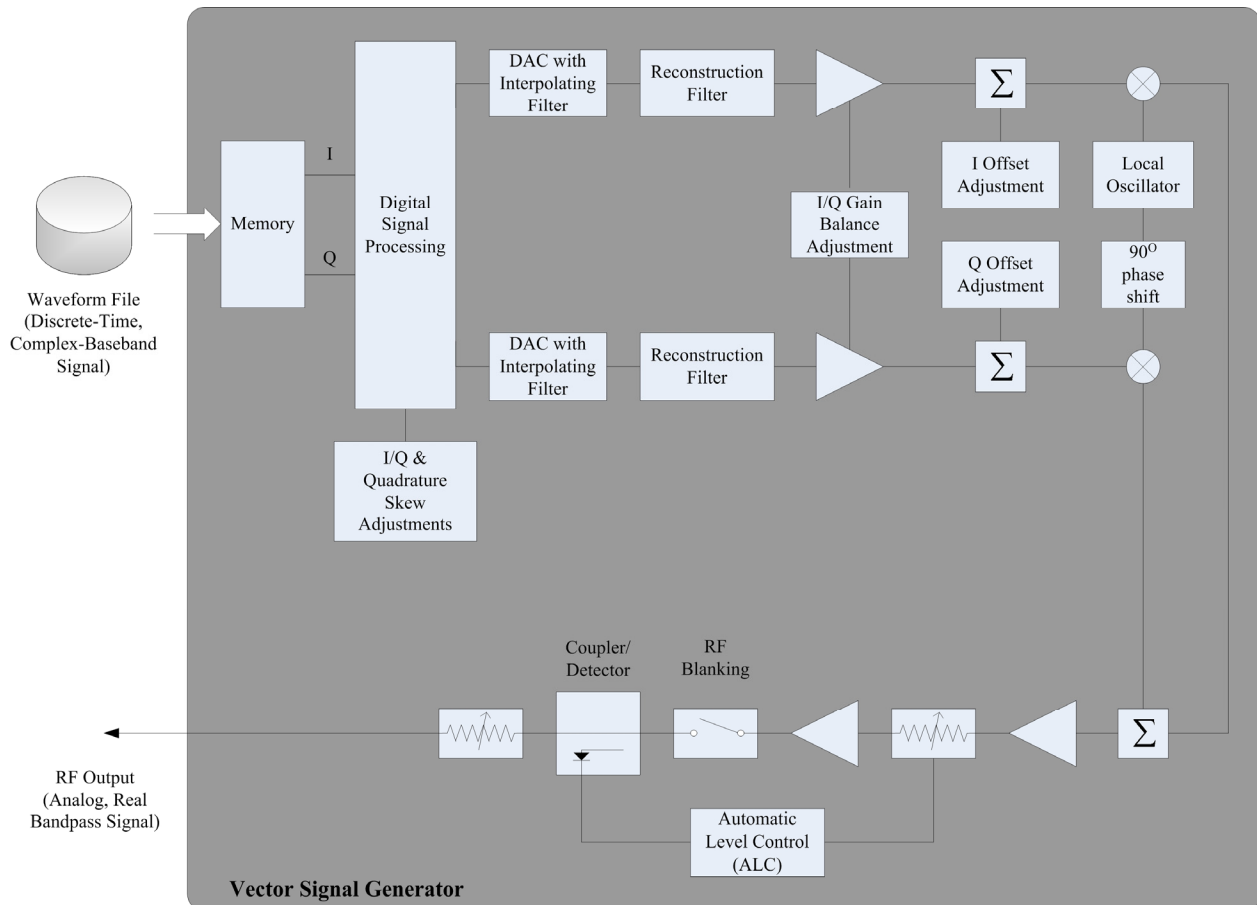


Figure B-1. Block diagram of the Vector Signal Generator.

The smoothed analog I signal at the output of the reconstruction filter modulates an LO while the corresponding Q signal modulates a 90° phase-shifted LO. These modulated signals are summed to produce a real bandpass signal centered at the LO frequency. After this, only the amplitude of the bandpass signal is adjusted.

Signal amplitude is dependent upon the settings for the automatic level control (ALC) and the RF output power. When the ALC is on, the ALC circuitry senses the RF output power and uses this level in a feedback loop to maintain the RF output power at a constant calibrated level. The ALC causes unwanted amplitude fluctuations in signals with variable amplitudes. Since the interference signals have amplitude variations, we chose to turn off the ALC.

## **B.2. Techniques to Optimize RF Output Performance**

Hardware I/Q modulation within the VSG generates undesirable signals as well as the desired waveform. Undesirable signals include local oscillator (LO) feed-through, intermodulation products, and other spurious responses. LO feed-through, produced by I and Q DC offset voltages within the I/Q modulator, is perhaps the most prominent unwanted signal. While generation of the undesirable signals is unavoidable, the amplitude of the undesirable signals can be minimized using various techniques including I/Q calibration, pre-distortion, RF blanking, and frequency shifting.

### **B.2.1. I/Q Calibration and Adjustments**

Effects of imperfect I/Q modulation are compensated for by adjustments to parameters that include I and Q DC offsets, I/Q gain balance, I/Q timing skew, and quadrature skew. I and Q DC offset adjustments vary the DC voltage of I and Q signals, respectively. I/Q gain balance adjustment varies the gain of the I signal relative to the gain of the Q signal. I/Q skew adjustment delays I relative to Q or vice versa. Quadrature skew changes the phase angle between I and Q signals.

I/Q adjustments can be made with custom or vendor-supplied internal I/Q adjustment routines. Custom routines consist of playing a test waveform through the VSG and monitoring its output on a spectrum analyzer (SA). Optimum I/Q modulation settings are found by repetitively adjusting the parameters and observing the effects of adjustment on the SA. For example, a two-tone test signal, played through the VSG, can be used to minimize LO feed-through. Optimum DC offset settings are found by repetitive adjustment of these settings and monitoring the amplitude of the LO feed-through on the SA. In contrast, vendor-supplied routines use internal test waveforms and monitoring functions.

Since both custom and vendor-supplied routines provided similar results, we chose the vendor-supplied routine to reduce development time and test-system complexity. To maintain the best-possible performance, we perform I/Q calibration before each DTV interference susceptibility test.

### **B.2.2. Waveform Pre-distortion**

Pre-distortion software is available from the manufacturer that can be used to further minimize the effects of I/Q modulator imperfections in addition to performing an I/Q calibration. This software requires that the VSG be connected to an Agilent PSA or ESA spectrum analyzer. The software then applies corrections to I and Q data to minimize undesirable signals as determined by automated measurements by the SA.

While this technique can provide superb results in minimizing undesirable signals, it has several limitations that preclude its use in our measurements. First, this technique requires monitoring the RF output of the VSG on a SA any time data correction is desired. This would add more complexity to the measurement system. Second, changing the settings on the VSG requires new corrections to be made on I and Q waveform data. Perhaps an even more serious limitation is that this technique can only be used with waveforms that use a sampling rate of 100 million samples per second (MSps). Many of the waveforms that we use have other sampling rates. For these reasons, we chose not to use pre-distortion.

### **B.2.3. RF Blanking**

RF blanking can be used to mitigate LO feed-through when the signal is known to be off. For our tests, this includes gating periods. RF blanking uses the pulse modulation circuitry in the VSG to turn off the RF output. The user generates a separate marker file that contains Boolean values corresponding to each data sample in the waveform file. Each Boolean value in the marker file instructs the pulse modulation circuitry to turn the RF output on or off while the corresponding data sample in the waveform is being played on the VSG. Using a marker file, the user can specify turning off the RF output whenever a waveform data sample is zero, thus squelching the LO feed-through that would normally be present in the RF output. The pulse-modulation circuitry used for RF blanking typically provides 80 dB of attenuation for the RF-off state.

Practical limitations associated with RF blanking prevented us from using it. Most importantly, there is a finite rise and fall time associated with the pulse modulation circuitry. Unfortunately, the rise and fall times can be as long as 10 nanoseconds, which is as long as the sample period. Consequently, RF blanking can modulate the desired signal. This modulation is most evident when there are numerous transitions between zero and non-zero voltages. Additionally, the VSG introduces a delay between the time a waveform file sample is played and when RF blanking occurs. This delay is on the order of 40 to 50 nanoseconds and varies from one VSG to another. The delay must be experimentally determined and incorporated into the marker file.

### **B.2.4. Frequency Shifting the Complex-Baseband Signal**

Another method of minimizing the effects of LO feed-through is to frequency shift the CBB signal by  $f_0$  during computer signal simulation so that the LO is outside the bandwidth of the desired signal as shown in Figure B-2.  $f_0$  should be chosen so that all significant spectral content of the desired signal is undistorted by the band edges of the VSG frequency response. If this

distortion is unavoidable, it can be mitigated to some extent by applying an inverse filter, which compensates for the VSG frequency response, to the waveforms during simulation. As demonstrated in Appendix C, LO feed-through was not a problem for the DTV interference susceptibility tests; hence, we chose not to frequency shift.

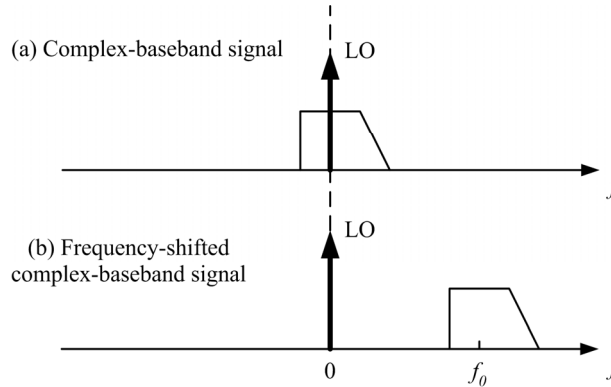


Figure B-2. Frequency shifting the complex-baseband signal by  $f_0$ .

### B.3. Waveform Conditioning

In this study, the simulated CBB waveforms of various interference signals are created and stored sequentially in a binary waveform file as a sequence of discrete-time, double-precision I and Q values. To be useful to the VSG, these values must be converted to a fixed-point format. This conversion process is performed in three steps: normalization, scaling, and quantization.

Normalization is accomplished by finding the maximum of the absolute values of all I and Q data values and dividing all the I and Q values by this maximum value. After normalization, all I and Q values are within the range  $-1 \leq \{I, Q\} \leq 1$ .

Scaling compensates for the effects of sample interpolation performed by the VSG prior to digital-to-analog conversion and reconstruction filtering. The interpolator, which runs at four times the AWG sample rate, often causes samples with large voltage transitions to exceed the range of the digital-to-analog converter (DAC). As recommended by the manufacturer and to ensure that DAC over-range errors do not occur, normalized I and Q data values are scaled by a factor of 0.7. After scaling, all I and Q values are within the range  $-0.7 \leq \{I, Q\} \leq 0.7$ . A less conservative scaling factor can be determined experimentally (on a signal by signal basis) by monitoring VSG DAC over-range error indicators.

Finally, I and Q floating point values are converted to fixed-point numbers corresponding to the DAC resolution. For a 16-bit DAC, normalized and scaled floating-point values are multiplied by  $(2^{15} - 1)$  and converted to 16-bit signed integer I and Q values. After quantization, all I and Q values are within the range  $-22,937 \leq \{I, Q\} \leq 22,937$ . Prior to loading the waveform into VSG RAM, it is important to resolve discrepancies between fixed-point formats that may exist between the computer, which processed the samples, and the VSG, which uses them. In our case,

samples are processed on a PC using an Intel processor and played on a VSG using a Motorola processor. This requires a conversion from little endian fixed-point format to big endian.

#### **B.4. Operating Procedures**

In this study, VSG operational procedures are controlled via software using SCPI commands. This permits highly repeatable operation. The sequence of commands used to setup and operate the VSG is provided below:

1. System Preset: Perform the same operation as the front panel Preset button. Set the VSG to the factory defined state.
2. Clear Status Register: Clear the status byte register including the error queue and all event registers.
3. ALC Off: Turn off automatic level control.
4. Set RF Frequency: Set LO frequency that the I and Q samples modulate.
5. Clear Waveform Memory: Delete WFM1 waveform memory (RAM) and wait 2 seconds before issuing the next command to allow deletion to complete.
6. Load Waveform File: Load normalized waveform file from personal computer into WFM1 waveform memory using FTP.
7. Select Waveform Segment: Select the waveform segment corresponding to file loaded into WFM1 waveform memory.
8. Set Sample Rate: Set sample rate according to that specified in simulation.
9. AWG On: Turn on baseband AWG and wait 10 seconds before issuing the next command to allow baseband reconfiguration.
10. Modulation On: Enable waveform modulation of LO.
11. Set Run-Time Scaling to 100%: The factory default is 70% and is only appropriate when loaded waveforms are not already properly normalized.
12. I/Q Calibration: Perform I/Q calibration.
13. Set RF Output Power Level.
14. RF On: Turn on RF output.

## APPENDIX C: EFFECTS OF VSG LO FEED-THROUGH ON DTV INTERFERENCE SUSCEPTIBILITY TESTS

This appendix provides a quantitative analysis of the effects of VSG LO feed-through on digital television (DTV) interference susceptibility tests.

### C.1. LO Feed-Through Inherent to DTV Systems

As described in *ETSI Measurement Guidelines for DVB Systems* [19] and shown in Figure A-1, unwanted LO feed-through is inherent to quadrature-amplitude modulated (QAM) DTV systems. Note that QPSK receivers being tested in this effort are a subset of QAM. LO feed-through is often characterized by a carrier suppression specification defined as

$$CS = \frac{P_{DTV}}{P_{LO}} \quad , \quad (C-1)$$

where  $P_{DTV}$  is the total power of the QAM signal without LO feed-through and  $P_{LO}$  is the power of the LO feed-through.

The signal has a noise equivalent bandwidth of  $B_{DTV}$ , which we assume is equal to the QPSK symbol rate,  $R_S$ . We also assume that the spectrum analyzer (SA) uses Gaussian-shaped filters whose noise equivalent bandwidth is approximately the resolution bandwidth ( $RBW$ ). Since the noise and the DTV signal are zero-mean random processes, the mean powers of each signal can be separated arithmetically. As a result, the noise, signal, and LO feed-through power as well as the carrier suppression ratio can be computed from SA measurements.

Various terms in the computation are used.  $PSD(f)$  refers to power spectral density in watts/Hz, which is, in general, frequency dependent.  $P$  refers to power in watts. Finally,  $M$  refers to a SA power measurement in watts. For this appendix,  $M$  is measured in 1-kHz  $RBW$  with root-mean-square (rms) detection and 0.3-second integration time (i.e., sweep time divided by number of frequency steps). Subscripts  $nSYS$ ,  $DTV$ , and  $LO$  refer to contributions from system noise, satellite DTV signal, and local-oscillator feed-through respectively.

$M_{nSYS}$  is average power of the system noise measured with the system signal path cascaded with the SA, as shown in Figure 20, but with the DTV signal turned off. Noise from the SA and LNB are included in the measurement and we assume it to be flat across the satellite channel. From this measurement, power density of the system noise is computed as

$$PSD_{nSYS}(f) = \frac{M_{nSYS}}{RBW} \quad .$$

$M_{DTV+nSYS}$  is the average power of the DTV signal plus system noise measured by the SA at frequency  $f_1$  slightly offset from the center frequency of the DTV signal but still in the region

where the DTV power spectral density is constant. The corresponding power spectral density without system noise is

$$PSD_{DTV}(f_1) = \frac{M_{DTV+nSYS}}{RBW} - PSD_{nSYS}(f) \quad .$$

Average power of the DTV signal is

$$P_{DTV} = PSD_{DTV}(f_1) \times B_{DTV} = PSD_{DTV}(f_1) \times R_s \quad .$$

$M_{LO+DTV+nSYS}$  is the average power of the LO feed-through plus DTV signal plus system noise measured by the SA centered on the DTV signal. From this measurement, power of the LO feed-through is computed as

$$P_{LO} = M_{LO+DTV+nSYS} - M_{DTV+nSYS} \quad .$$

Carrier suppression is computed from  $P_{LO}$  and  $P_{DTV}$  with equation C-1.

Figure C-1 shows LO feed-through generated by the satellite simulation subsystem, described in Section 4.4, and measured by the spectrum analyzer. Satellite simulator power was set so that  $SNR$  was approximately 8.5 dB – the lowest  $SNR$  tested and therefore the most susceptible to LO feed-through from the VSG. The following measurements were made:  $M_{nSYS} \approx -90.5$  dBm,  $M_{DTV+nSYS} \approx -82.0$  dBm,  $M_{LO+DTV+nSYS} \approx -71.6$  dBm. Calculations from these measurements give  $P_{LO} \approx -72.2$  dBm,  $P_{DTV} \approx -38.6$  dBm, and  $CS \approx 34$  dB. Note that these results are given in dB, but the calculations were performed in linear units.

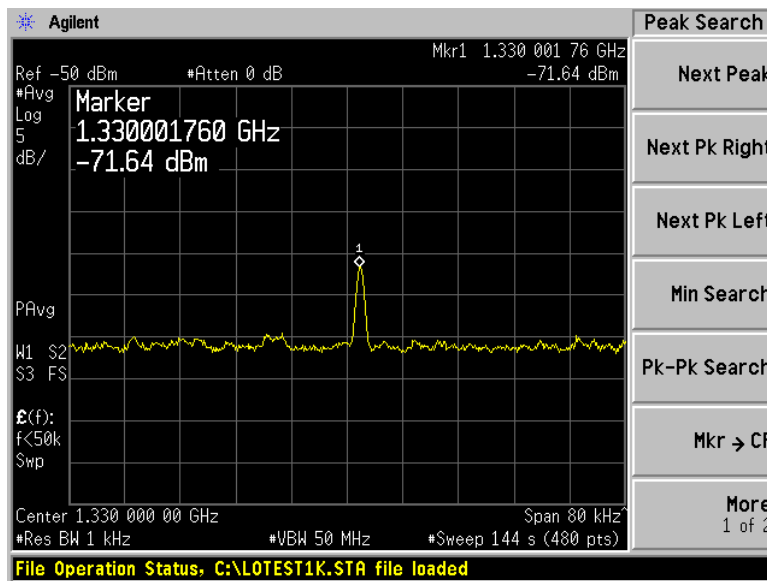


Figure C-1. LO feed-through from satellite signal generator.

## C.2. Experiment

Satellite receivers that demodulate QPSK signals are designed to tolerate reasonable levels of LO feed-through. However, it is not clear how much additional LO feed-through, introduced by the VSG-generated interference signals in our DTV interference susceptibility test, can be tolerated.

Figure C-2 depicts hardware used to emulate the VSG as it is used during DTV interference susceptibility testing to generate gated-noise signals from simulated waveforms. The noise diode, amplifier, and high-speed switch generate a gated-noise signal, while the signal generator adds a CW signal that emulates the VSG LO feed-through.

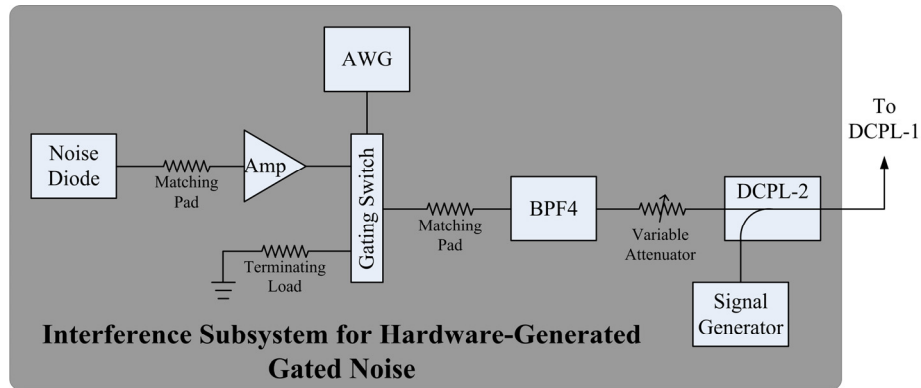


Figure C-2. Interference subsystem for testing the effects of LO feed-through.

The measurement procedure consisted of the following four steps:

1. **Baseline signal-quality measurement:** The satellite simulation subsystem was set to 8.5-dB *SNR*. Baseline interference, i.e., hardware-generated gated noise, was coupled into the test system at directional coupler DCPL-1 (see Figure 20) at a level that caused the segment error rate (*SER*) to be approximately  $10^{-4}$ . Baseline signal quality was recorded.
2. **Baseline-plus-CW signal-quality measurement:** A CW signal was introduced at directional coupler DCPL-2 and signal quality was recorded with the DTV receiver exposed to baseline-plus-CW interference. The CW signal was centered in the DTV channel at 3820 MHz and increased in 5-dB steps. The baseline-plus-CW measurements were stopped at a CW level that caused *SER* to exceed  $10^{-2}$ .
3. **Baseline and baseline-plus-CW power measurement:** The CW amplitude was set to the highest level that did not cause signal quality to deviate from the baseline signal quality. SA measurements at the CW frequency and offset from the CW frequency were made at the output of the LNB in 1-kHz *RBW*. Calculations using these measurements determined the amount of CW power alone. Figure C-3(a) shows SA measurements of hardware-generated baseline-plus-CW Gaussian noise interference (GN-01).

4. VSG interference and LO feed-through power measurement: The hardware-generated interference subsystem was replaced by the VSG loaded with the same corresponding gated-noise waveform. VSG amplitude was adjusted so that the gated-noise power, away from the LO frequency, matched the baseline power measured previously. SA measurements at the LO frequency and offset from the LO frequency were made at the output of the LNB in 1-kHz *RBW*. Calculations using these measurements were used to determine the amount of LO feed-through power alone. Figure C-3(b) shows SA measurements of VSG-generated Gaussian noise interference (GN-01).

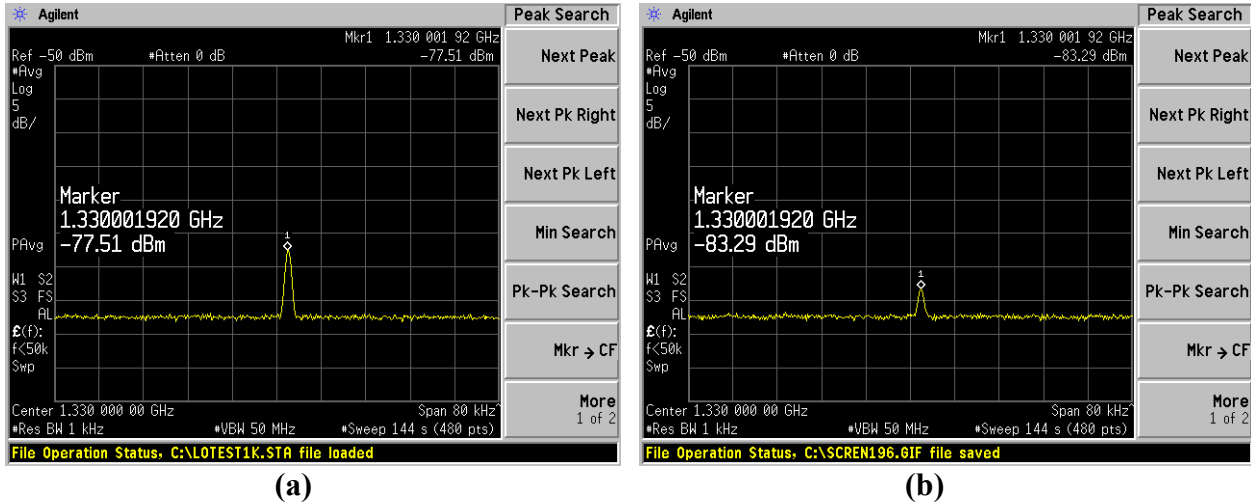


Figure C-3. SA measurements of (a) hardware-generated Gaussian-noise plus CW and (b) VSG-generated Gaussian noise with LO feed-through.

### C.3. Results

Interference permutations considered for this experiment were continuous Gaussian noise (GN-01), gated noise with 100-nanosecond on time and 50% duty cycle (GN-07), and gated noise with 100-nanosecond on time and 6.25% duty cycle (GN-09). VSG-generated GN-09 has the strongest LO feed-through relative to the intended-interference power. This is because gating attenuates the noise average power but has no effect on the LO feed-through power. In fact, GN-09 LO feed-through will be the strongest encountered out of all gated-noise interference permutations listed in Section 2.1.5 because the VSG amplitude has to be set higher to create an  $SER = 10^{-4}$  condition.

Figures C-4 – C-6 display best estimates of four DTV signal quality metrics, i.e., segment error rate (*SER*), pre-Viterbi bit error rate (*BER*), modulation error rate (*MER*), and error vector magnitude (*EVM*). These metrics are plotted against increasing levels of CW power representing VSG LO feed-through. Systematic error, introduced by the measurement system, has been mostly removed from these results. LO feed-through of the satellite simulator (black) and VSG (red) are plotted as vertical lines. Signal quality metrics began to degrade at CW powers of -60 dBm, -62 dBm, and -65 dBm for GN-01, GN-07, and GN-09 respectively.

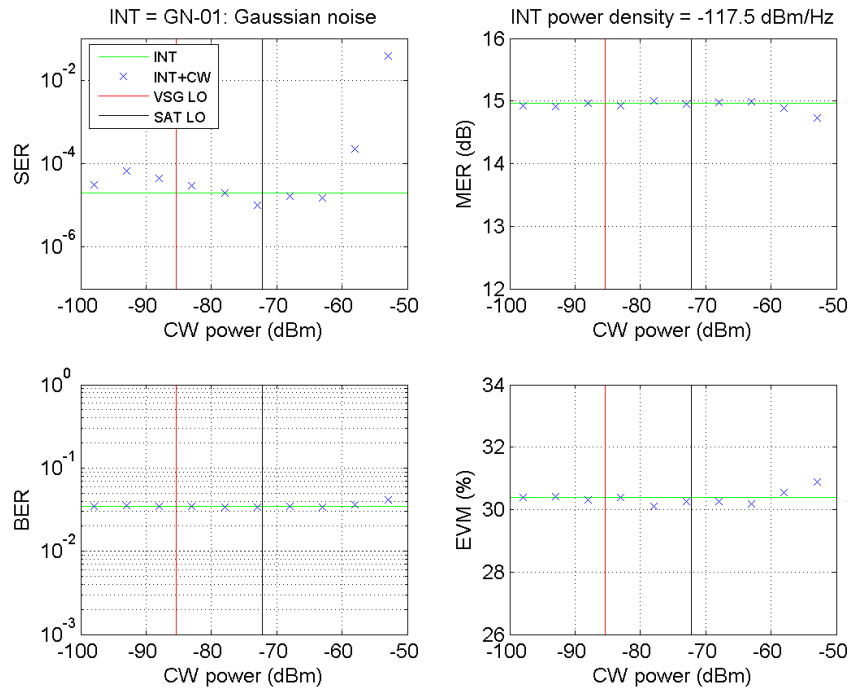


Figure C-4. LO feed-through measurements for Gaussian noise interference.

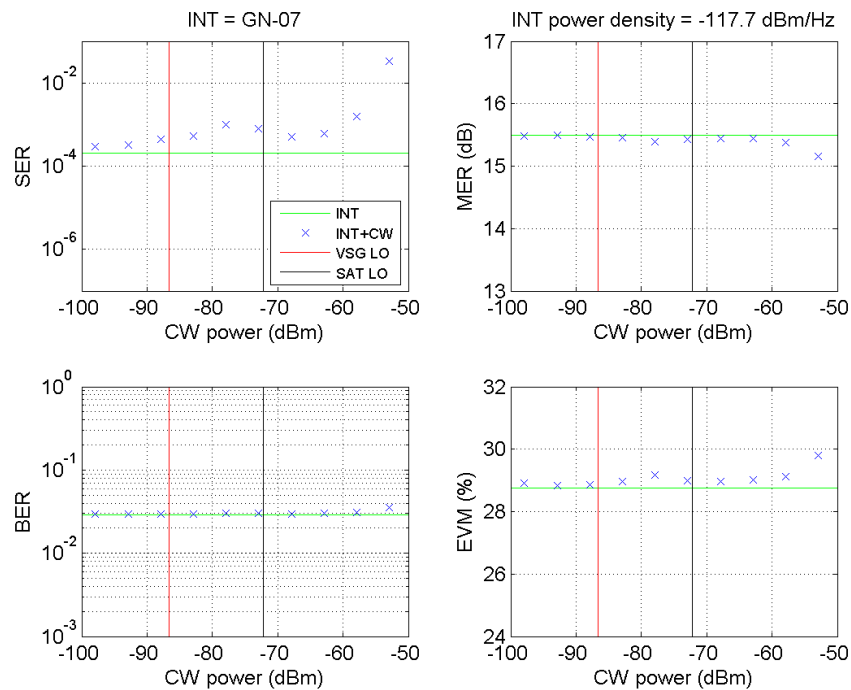


Figure C-5 LO feed-through measurements for gated noise interference with a 100-nanosecond on-time and 25% duty cycle.

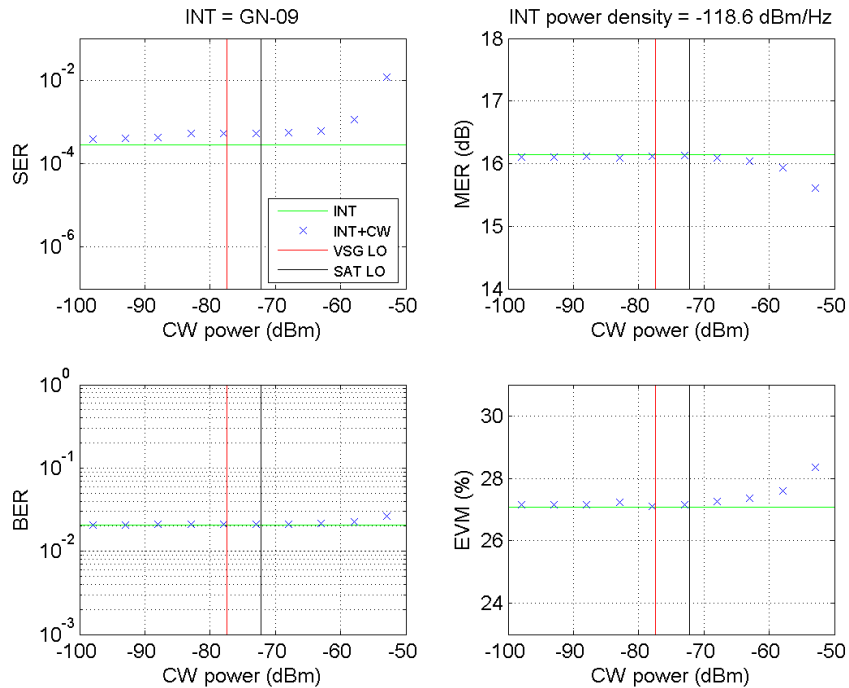


Figure C-6. LO feed-through measurements for gated noise interference with a 100-nanosecond on-time and 6.25% duty cycle.

#### C.4. Effect of VSG LO Feed-Through on Carrier-Suppression Ratio

The vertical red and black lines in Figure C-4 – C-6 show that LO feed-through of the satellite simulator and VSG were lower than the threshold where DTV quality metrics began to degrade. However, it is the combination of these residual carriers that we are concerned with. Figure C-7 shows how the combination of LO feed-through powers degrade CS from 34 dB.

The highest VSG LO feed-through for the gated-noise signals listed in Section 2.1.5 is approximately  $-74 \text{ dBm} = -77 + 3 \text{ dBm}$ , where  $-77 \text{ dBm}$  is the LO feed-through power of the VSG generating GN-09 at a level that causes  $SER$  to be  $10^{-4}$  (illustrated in Figure C-6) and  $3 \text{ dB}$  is a conservative estimate of the additional interference power needed to bring that  $SER$  to  $10^{-1}$ . Figure C-7 shows that this degrades carrier suppression to approximately  $32 \text{ dB}$ ; this is the minimum CS for the gated-noise interference potential study. In other words, all gated-noise interference signals generated in this study will have a  $CS \geq 32 \text{ dB}$ .

Results in Section C.3 show that, in the worst-case, DTV signal quality metrics began to degrade at an LO feed-through level of  $-65 \text{ dBm}$ , which degraded carrier suppression to approximately  $26 \text{ dB}$ . Therefore, as shown in Figure C-7 there is a  $6\text{-dB}$  margin between the measured CS threshold and the minimum CS for the gated-noise interference potential study.

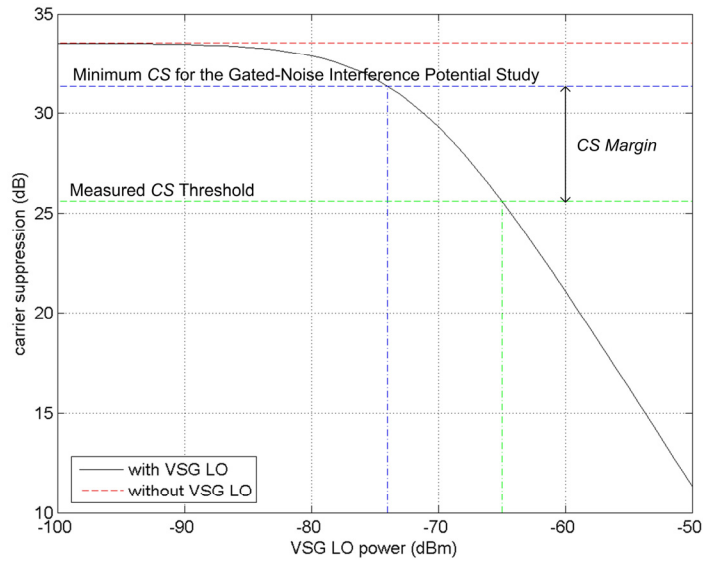


Figure C-7. Effects of VSG LO on carrier suppression.

### C.5. Conclusion

This experiment shows that the highest VSG LO feed-through power, -74 dBm, for all gated-noise interference signals generated in this study degrades the carrier suppression ratio from 34 to 32 dB. This is approximately 6 dB above the carrier suppression ratio that degraded signal quality metrics for a DTV receiver operating at  $SER \approx 10^{-4}$ . Hence, VSG LO feed-through is not a problem for our DTV interference susceptibility tests.

## APPENDIX D: ESTIMATING AND GRAPHING THE AMPLITUDE PROBABILITY DISTRIBUTION OF COMPLEX-BASEBAND SIGNALS

The amplitude probability distribution (*APD*) function has been found to be useful in characterizing signals and evaluating effects of interference on victim receivers. The following discussion defines the *APD* mathematically and demonstrates how it can be estimated and plotted with the MATLAB<sup>®</sup> language.

### D.1. Estimating the *APD*

The mathematics and terminology of the *APD* are based on the concept of random variables. A random variable is a function,  $X$ , which assigns a real number,  $X(v)$ , to every element,  $v$ , of a sample space. In our case, the random variable assigns a real number representing the amplitude of a complex-baseband signal drawn from a sample space via signal simulation or measurement. The *APD* is expressed as

$$F(a) = \wp(X(v) > a)$$

or more commonly

$$F(a) = \wp(X > a) \quad ,$$

where  $a$  is an amplitude value and  $\wp(\ )$  means probability.

A discrete estimate of the *APD* can be obtained from a finite set of samples. This is accomplished by sampling the complex-baseband signal  $N$  times, converting these samples to the amplitudes

$$a(n) \quad , \quad n = 1, 2, \dots, N \quad ,$$

ordering the amplitudes from smallest to largest

$$a[n] \quad , \quad n = 1, 2, \dots, N \quad ,$$

where the square brackets distinguish the ordered amplitudes from the unordered amplitudes, and computing

$$\wp(X > a[n]) = 1 - \frac{n}{N} \quad .$$

The routine “[a, p] = apd(s)” (given in Appendix D.5) estimates the *APD* from  $N$  amplitude samples. Elements in the vector “s” are checked to make sure they are amplitudes, i.e., that they are real and positive. “s” is ordered from smallest to largest via “a = sort(s)”, where “sort” is a MATLAB function, and corresponding probabilities are computed via “p = 1-(1 : N)/N”.

## D.2. Plotting the *APD*

*APDs* are typically displayed on a Rayleigh graph whose axes are transformed by functions that linearize the *APD* of the Rayleigh-distributed amplitudes of complex Gaussian noise. Derivation of these functions begins with the expression of the *APD* of a Rayleigh-distributed random variable

$$\wp(X > a) = \exp\left(\frac{-a^2}{\sigma^2}\right) ,$$

where  $\sigma$  represents the standard deviation of zero-mean complex noise. This function is linearized by the natural logarithm function and converted to decibels by

$$10 \log(a^2) = 10 \log(\sigma^2) + 10 \log(-\ln(\wp(X > a))) .$$

Graphical coordinates,  $x$  and  $y$ , are introduced by

$$y = \log(a^2)$$

and

$$x = 10 \log(-\ln(P_0)) - 10 \log[-\ln(\wp(X > a))] ,$$

where  $P_0$  is the probability at the graph origin.

The  $x$ -axis is in units of percentage and labeled “percentage of time ordinate is exceeded” or “percent exceeding ordinate.” The  $x$ -axis probabilities generally range from 0.0001 to 99 percent for problems associated with modern receiver design.

Signals are often normalized. Common normalization factors are the root-mean-square (rms) voltage of the signal or the rms voltage of white Gaussian noise. If normalized by the rms voltage of the signal, the  $y$ -axis is labeled “dB relative to rms voltage” or “dB relative to average power.” If normalized by the rms voltage of white Gaussian noise, the  $y$ -axis is labeled “dB relative to measurement system average noise power” or “dB relative to  $kTB$ .” Otherwise, units appropriate to the samples such as dBV or dBW are used.

The routine “plotapd(a,p)” plots the *APD* on a Rayleigh graph. The routine begins by checking for zero amplitudes and probabilities that will generate log function error messages. Zero amplitudes are possible for signals simulated without added noise. The largest or peak amplitude of the *APD* estimate is assigned zero probability. “Plotapd” circumvents these problems by replacing the zero value with the MATLAB constant “not a number” (NaN). The MATLAB “log” or “log10” functions will not generate error messages when operating on NaNs and the MATLAB “plot” routine will not plot points in which the abscissa or ordinate is NaN. The remainder of the routine transforms data and axes to the graphical coordinate system using the equations for  $x$  and  $y$  above.  $y$ -axis labeling is dependent on how or if the samples were normalized and therefore is left outside the plotting routine.

### D.3. Testing the Routines

The routine “testapd” demonstrates the use of the “apd” and “plotapd” routines by checking the median and mean values of two test signals (corresponding plots are shown in Figures D-1 and D-2). The first test signal is a ten-thousand element vector of linearly increasing voltages ranging from 0 to 9999. The median (i.e., the amplitude exceeded by 50 percent of the samples) of this signal is 5000 V or 74.0 dBV. The second test signal is a one-million element vector of complex Gaussian noise voltages with zero mean and a variance of  $2 V^2$ . The rms voltage is equal to the square root of the variance or 3.0 dBV. The corresponding probability is equal to  $1/e$  or 0.367 and expressed on the graph as 36.7%.

### D.4. Additional Comments

Several important amplitude statistics, including rms voltage or average power, can be computed with the information found in the *APD*. However, the *APD* cannot provide information concerning the signal time-domain behavior without other a priori information such as knowing that it is a periodically pulsed signal.

Additionally, the *APD* is strongly affected by the type of band-limiting filter; the *APD* estimate accuracy and precision are dependent on the sample interval and number of samples used. Consequently, these parameters should be documented with the *APD* graph.

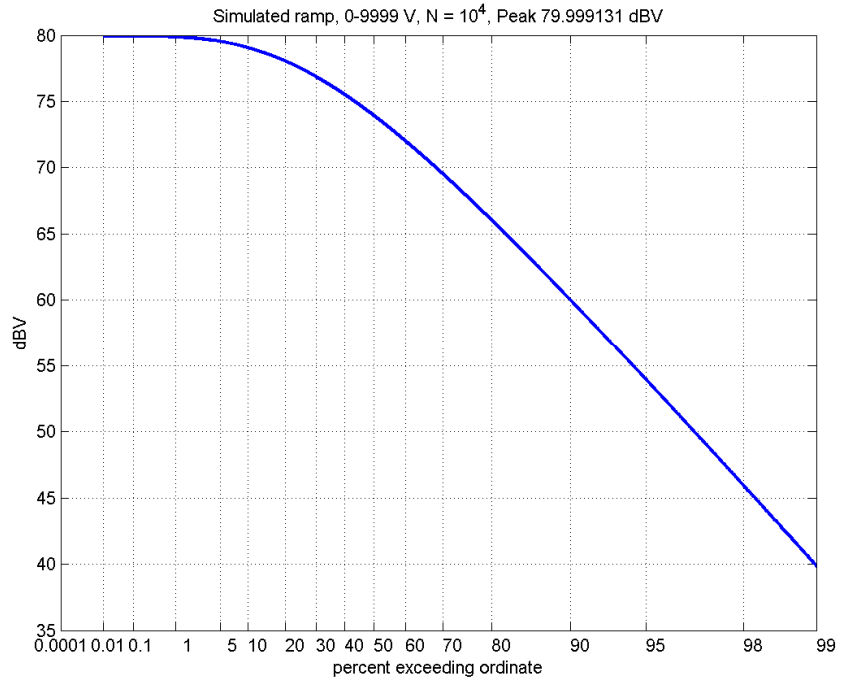


Figure D-1. *APD* of a ramp function increasing from 0 to 9999 V.

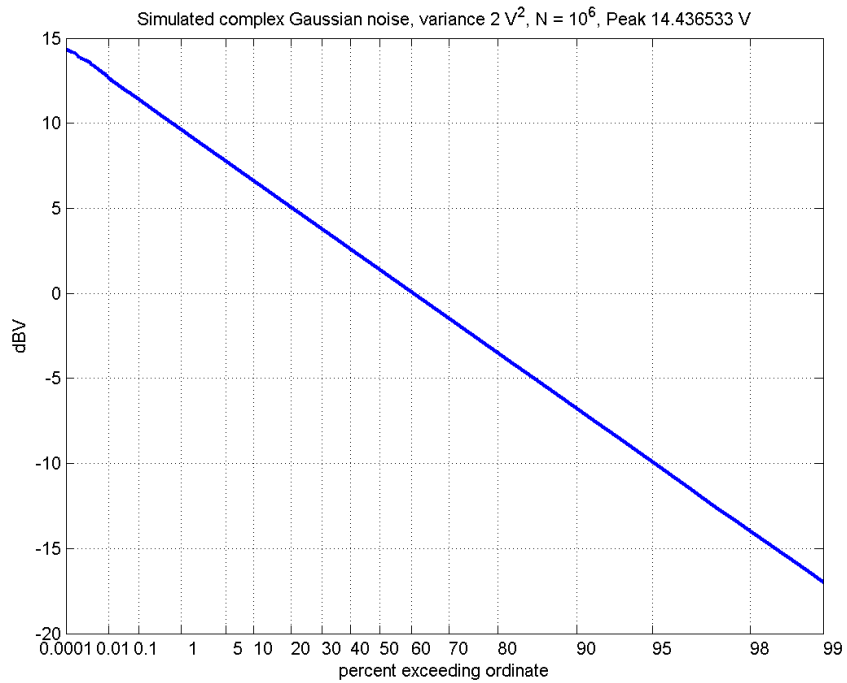


Figure D-2. *APD* of complex Gaussian noise with mean = 0 V and variance =  $2 V^2$ .

## D.5. MATLAB Code

### D.5.1. testAPD.m

```
% testAPD
% demonstrates how to use apd(s) and plotapd(a,p).

% ramp
N = 10.0^4;
v = [0:N-1];
[a,p] = apd(abs(v));
plotapd(a,p);
title(sprintf('Simulated ramp, 0-9999 V, N = 10^4, Peak %f dBV',20*log10(a(N))))
ylabel('dBV')
pause

%complex Gaussian noise
N = 10.0^6;
v = randn(1,N) + i*randn(1,N);
[a,p] = apd(abs(v));
plotapd(a,p);
title(sprintf('Simulated complex Gaussian noise, variance 2 V^2, N = 10^6, Peak %f
V',20*log10(a(N))))
ylabel('dBV')
```

### D.5.2. apd.m

```
function [a, p] = apd(s);
% [a, p] = apd(s) estimates the amplitude probability distribution function.
%
% input parameters:
% s = amplitude samples
%
% return variables:
% a = ordered amplitudes
% p = probability that the ordered amplitude is exceeded

if isreal(s) & min(s)>=0
    a = sort(s);
    N = length(a);
    p = 1 - [1:N]/N;
else
    disp('Input values must be amplitudes i.e. real and positive values.');
```

### D.5.3. plotapd.m

```
function plotapd(a,p)
% plots (a,p) pairs representing the APD on Rayleigh graph.
%
% input variables:
% a = ordered amplitudes
% p = probability of ordered amplitude

% x-axis labels (labels must be same length)
xticklabel = ['0.0001'; 0.01; 0.1; 1; 5; 10; 20; 30; 40; 50; 60; 70;
80; 90; 95; 98; 99];
ptick = [0.0001 .01 0.1 1 5 10 20 30 40 50 60 70 80 90 95 98 99]/100;
porigin = ptick(1);

% replace 0 valued amplitudes with NaN to avoid logarithm error messages
if min(a) == 0
    idx = find(a==0);
    a(idx) = NaN;
end

% replace peak amplitude 0 probability with NaN to avoid logarithmic error messages
p(length(a)) = NaN;

% map a and p and plot
x = 10.0*log10(-log(porigin)) - 10.0*log10(-log(p));
y = 20.0*log10(a);
plot(x,y,'LineWidth',2);
grid

% customize x axis
xlabel('percent exceeding ordinate');
xtick = 10.0*log10(-log(porigin))-10.0*log10(-log(ptick));
xLim([min(xtick) max(xtick)]);
set(gca,'XTick',xtick);
set(gca,'XTickLabel',xticklabel);

return
```

## APPENDIX E: DYNAMIC RANGE OF THE VECTOR SIGNAL ANALYZER

Statistics such as average power, amplitude probability distribution (*APD*), and power spectral density are measured with the vector signal analyzer (*VSA*) in this study. Accurate estimates of these statistics require the amplitudes of measured signals to lie within the dynamic range of the *VSA*. This appendix describes how average powers of measured signals are set to ensure accurate *VSA* measurements. First, a continuous wave (*CW*) dynamic range measurement is described. Next, average power measurements of four fundamental signals with differing peak-to-average power ratios (*P/A*) are described, and *APD* measurements of these signals are provided. Finally, guidelines for setting the average power of measured signals are given.

Four fundamental signals are considered in this appendix: *CW*, Gaussian noise, power-Rayleigh noise [20] with an exponent of 4, and a periodic pulse train with a 1-MHz pulse repetition frequency (*PRF*). All signals, including *CW*, were simulated in complex baseband (*CBB*) at a sample rate of 100 million samples per second (*MSps*), loaded into the *VSG* memory, upconverted to 3820 MHz, and applied to the input of the *VSA*. A power meter was used to verify average signal power applied to the input of the *VSA*. The *VSA* center frequency and input range were set to 3820 MHz and -30 dBm, respectively, and measurements were made in 36- and 3-MHz *VSA* spans.

### E.1. Dynamic Range Measurement

Dynamic range was measured by applying incrementally stronger *CW* signals to the *VSA* and recording amplitude estimates. The *CW* signal was generated with the vector signal generator (*VSG*) and connected to the *VSA* with a coaxial cable. *VSA* measurements were performed at increasing power levels in 2-dB steps. The initial input level was well below the noise floor of the *VSA* and the highest amplitude level was above its 1-dB compression point. Power levels where *VSA* overload occurred were noted.

Blue curves in Figures E-1 and E-2 show results from the dynamic range measurements. Average power computed from *VSA* samples is reported as “measured power” and average power measured by the power meter at the *VSA* input is reported as “input power.” *VSA* overdrive occurred at the same input power for both spans. The noise floor in the 36-MHz span, i.e., -77 dBm, is approximately 11 dB higher than the noise floor in the 3-MHz span, i.e., -88 dBm, which corresponds to the difference in bandwidths.

For the purposes of this study, dynamic range is defined as the straight portion of the *CW* curves in Figures E-1 and E-2. It is approximately 50 dB and 60 dB for the 36- and 3-MHz *VSA* spans.

### E.2. Average Power Measurements of Fundamental Signals

The dynamic range measurement procedure was repeated for Gaussian noise, power-Rayleigh noise, and a periodic pulse train. Results are plotted in Figures E-1 and E-2; the periodic pulse train is denoted by the acronym *UPS*, which stands for uniform pulse spacing. As shown in Table

E-1, VSA overload occurred at the lowest average power for power-Rayleigh noise, next for the periodic pulse train, and last for Gaussian noise. All occurred well below the CW overload. Interestingly, the measured power departed from the straight, top-portion of the CW curve at varying input powers. All measured powers departed from the straight, bottom-portion of the curve at the same input power, i.e., approximately -70 dBm and -80 dBm for the 36- and 3-MHz VSA spans, respectively.

Table E-1. Minimum Input Power of Signals Causing VSA Overload (dBm)

VSA Span	36 MHz	3 MHz
CW	-20	-20
Gaussian Noise	-32	-42
Power-Rayleigh	-48	-57
1-MHz Pulse Train	-32	-43

### E.3. *APD* Measurements of Fundamental Signals

Next, *APDs* were calculated from the VSA measurements performed previously and plotted in Figures E-3 through E-10. These plots show how the choice of average power affects *APD* measurement accuracy, which is made evident by accurate replication of *APD* features. For example, peak features were poorly replicated when strong amplitudes caused amplifier compression. Table E-2 shows the range of average powers where *APDs* were measured accurately. Each signal has a distinct P/A, defined as the power present 0.01% of the time divided by the average power. Gaussian noise P/A is approximately 10 dB, and CW P/A is 0 dB. Unlike Gaussian-noise and CW P/A, power-Rayleigh and periodic-pulse P/A are dependent on the measurement bandwidth. Table E-2 gives P/A measured in 36- and 3-MHz VSA spans.

Table E-2. Information from *APDs* Measured by the VSA

VSA Span	Input Power Range where <i>APDs</i> were Measured Accurately (dBm)		P/A (dB)	
	36 MHz	3 MHz	36 MHz	3 MHz
CW	-40/-20	-50/-20	0	0
Gaussian Noise	-63/-33	-73/-43	10	10
Power-Rayleigh	-63/-43	-84/-54	21	15
1-MHz Pulse Train	-53/-33	-64/-34	15	4

### E.4. Conclusion

Results show that the average input power of signals measured by the VSA should be determined from careful consideration of VSA dynamic range and characteristics of the signal. Failure to do so will result in inaccurate average power and *APD* estimates. As a guideline for VSA signal characterization measurements, the average power of the measured signal should be set 20 - 25 dB above the bottom of the VSA dynamic range. Using this guideline, average powers of

measured signals were set to -45 dBm and -55 dBm for 36- and 3-MHz VSA spans, respectively. Signals with higher P/A than those used in this appendix can be accurately measured by reducing the average power accordingly.

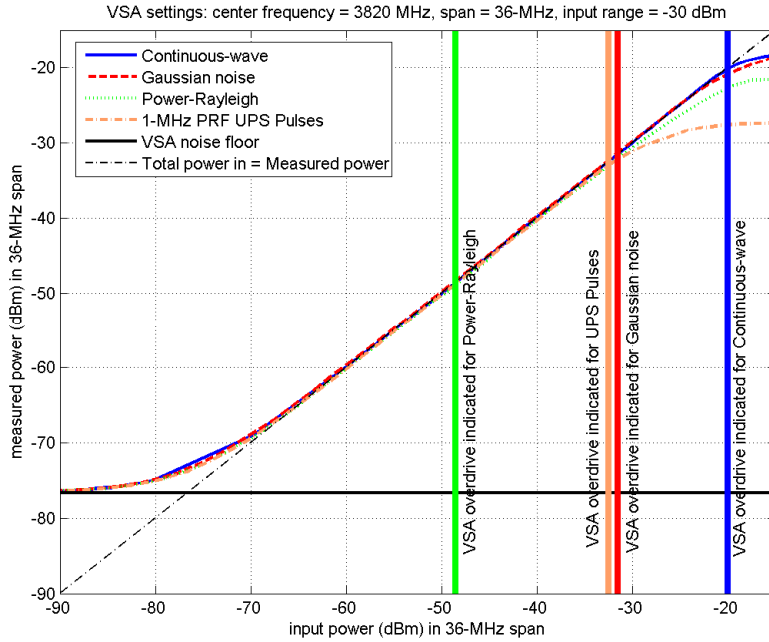


Figure E-1. Measured average power versus input average power of the VSA at span = 36 MHz.

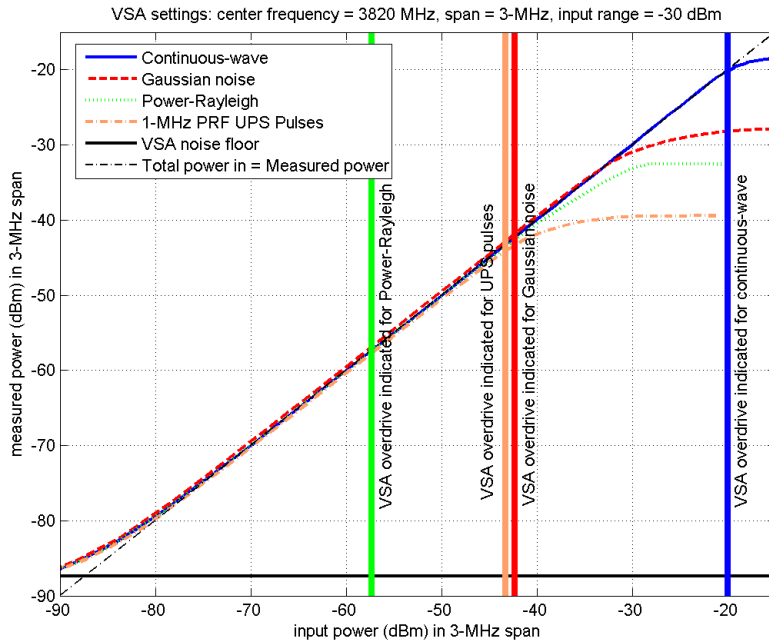


Figure E-2. Measured average power versus input average power of the VSA at span = 3 MHz.

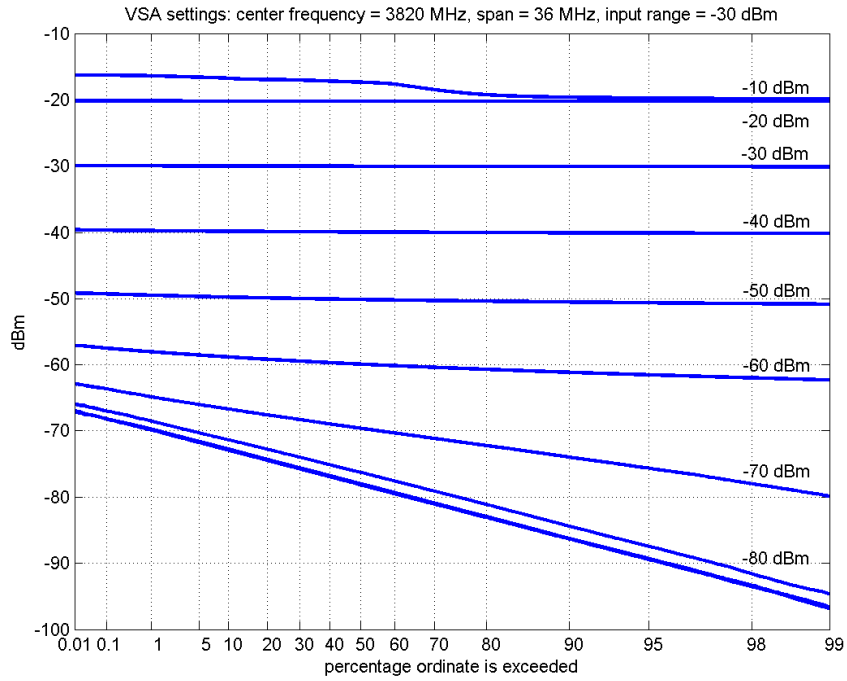


Figure E-3. *APDs* of continuous-wave signals at decreasing power levels. Average power at VSA input is shown at right edge.

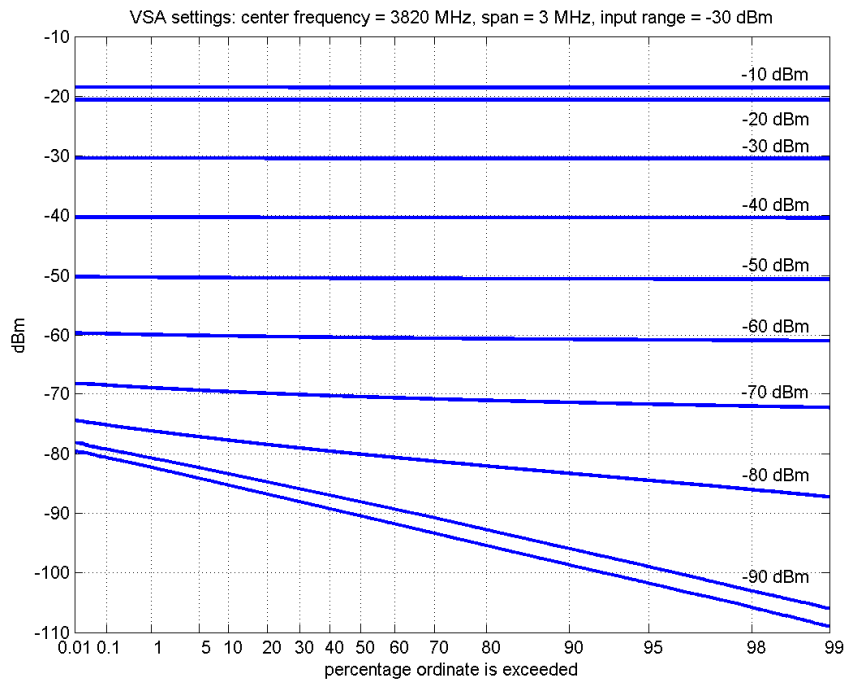


Figure E-4. *APDs* of continuous-wave signals at decreasing power levels. Average power at VSA input is shown at right edge.

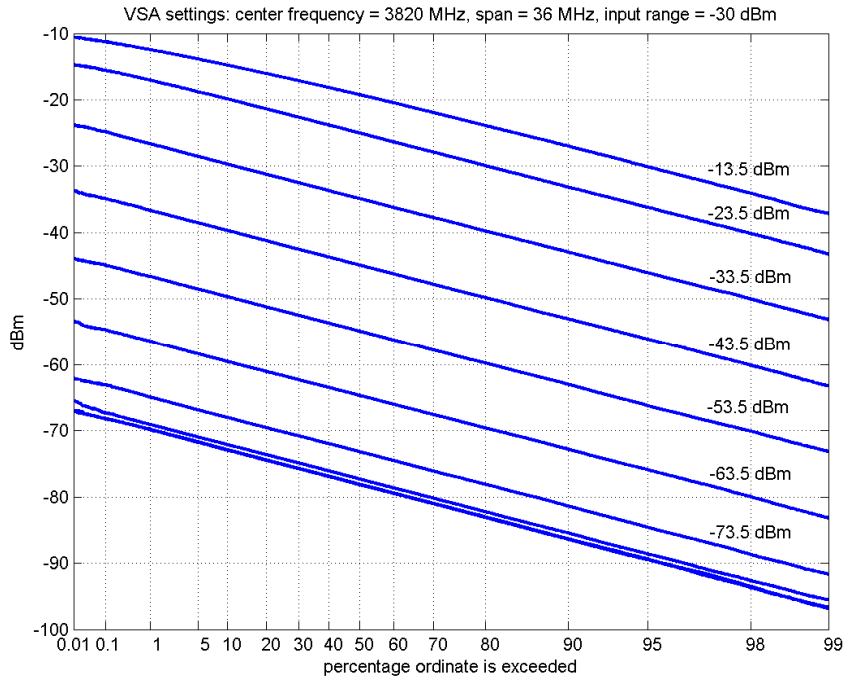


Figure E-5. *APDs* of Gaussian noise at decreasing power levels. Average power at VSA input in 36-MHz span is shown at right edge.

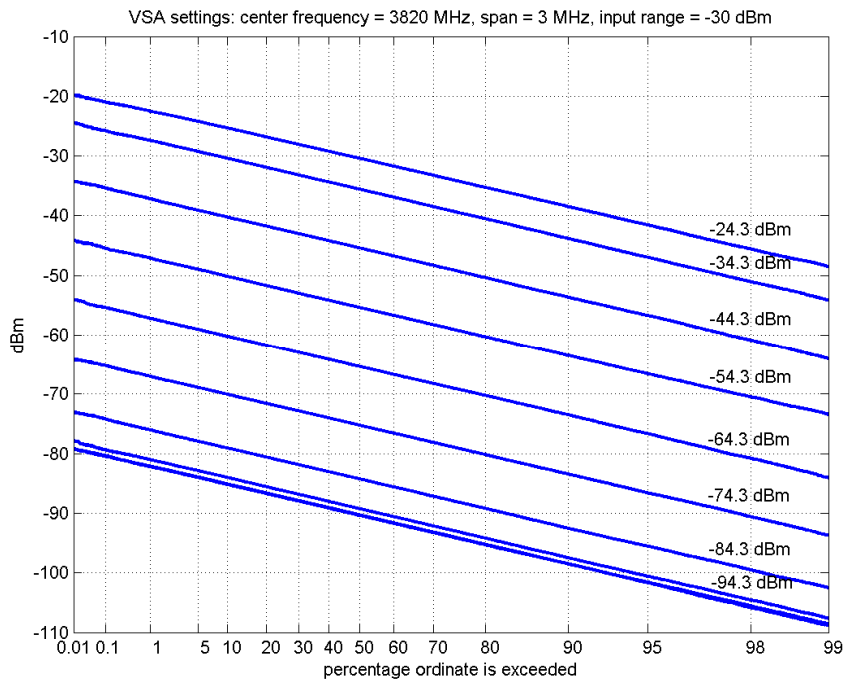


Figure E-6. *APDs* of Gaussian noise at decreasing power levels. Average power at VSA input in 3-MHz span is shown at right edge.

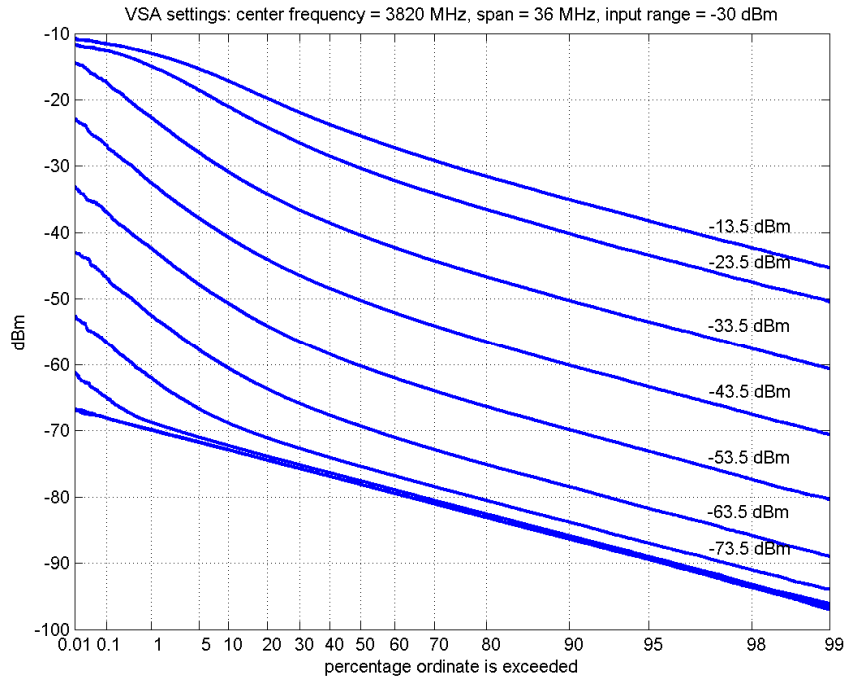


Figure E-7. *APDs* of power-Rayleigh signals at decreasing power levels. Average power at VSA input in 36-MHz span is shown at right edge.

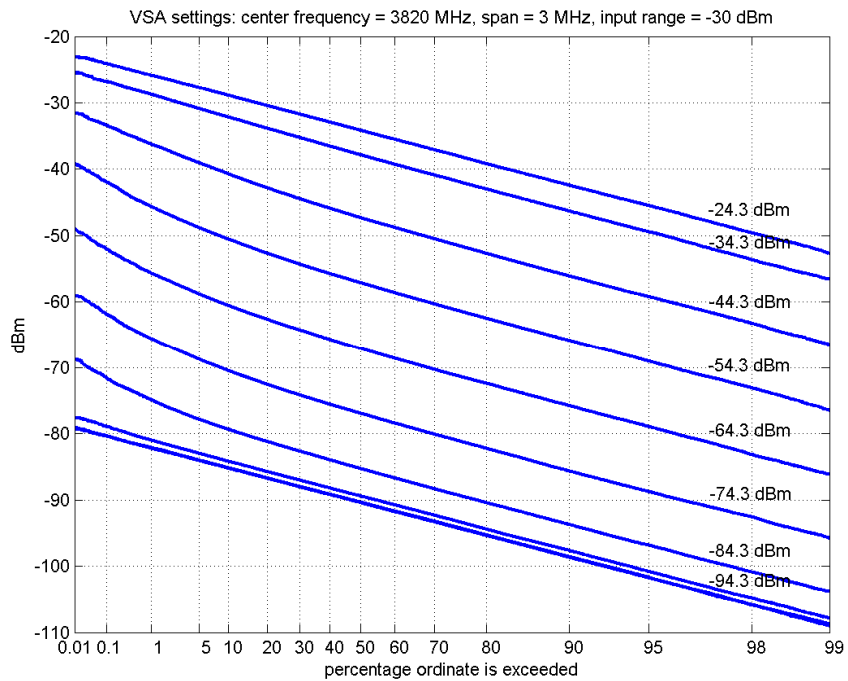


Figure E-8. *APDs* of power-Rayleigh signals at decreasing power levels. Average power at VSA input in 3-MHz span is shown at right edge.

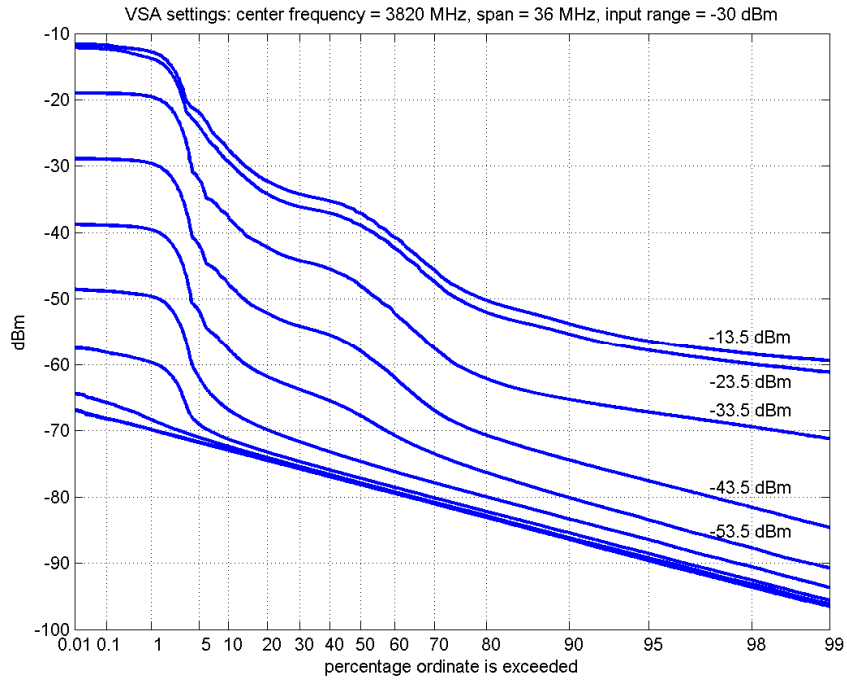


Figure E-9. *APDs* of 1-MHz PRF, uniform-pulse spaced pulses at decreasing power levels. Average power at VSA input in 36-MHz span is shown at right edge.

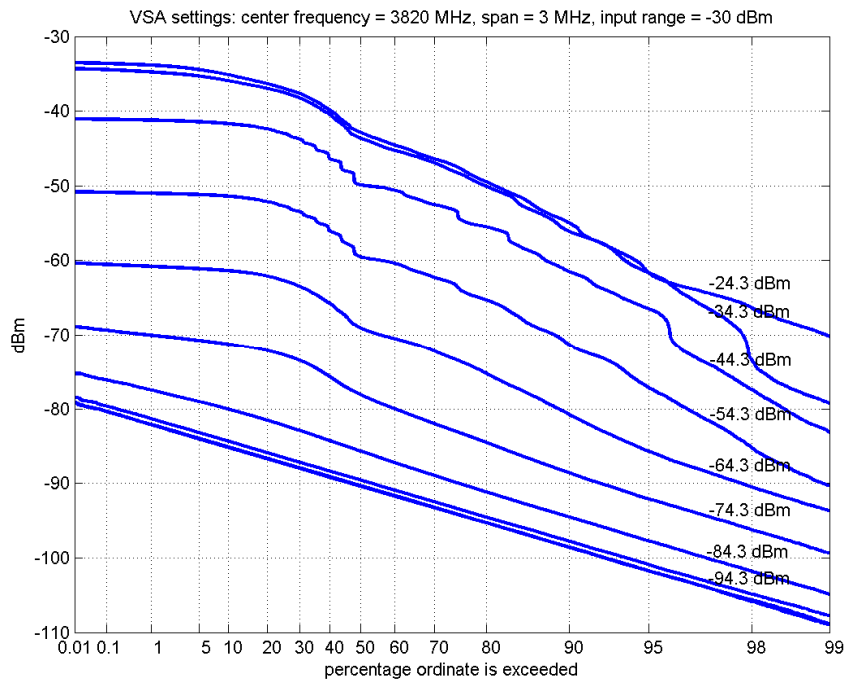


Figure E-10. *APDs* of 1-MHz PRF, uniform-pulse spaced pulses at decreasing power levels. Average power at VSA input in 3-MHz span is shown at right edge.

## APPENDIX F: TEST SYSTEM CHARACTERIZATION

This appendix provides characterization measurements and analyses of various parts of the DTV interference susceptibility test system.

### F.1. Characterization of the Signal Paths

The interference and satellite signal paths of the DTV interference susceptibility test system, shown in Figure 20, were characterized by gain, 1-dB compression point, noise figure, and frequency response. The interference signal path is defined from the interference signal input of directional coupler DCPL-1 to the input of the vector signal analyzer (VSA), and the satellite signal path is defined from the satellite signal input of DCPL-1 to the input of the VSA.

Gain and 1-dB compression point were measured using a continuous-wave (CW) input signal at 3820 MHz. The input compression point is expressed as an average power at the input of DCPL-1. The output compression point is defined at the VSA input and expressed as an average power and corresponding peak voltage. Peak voltage, expressed as

$$V_{peak} = \sqrt{2 \times 50 \times 10^{(P_{dBm} - 30)/10}} ,$$

is commonly used by the VSA and can be measured with an oscilloscope at the VSA input. Noise figures of both the interference and satellite signal paths were measured using a noise diode and spectrum analyzer according to the Y-Factor Method as described in [21].

Table F-1 summarizes the results for both interference and satellite signal paths. Note that the measurements of the output 1-dB compression point for both signal paths are within 0.1 dB. Within the precision of the measurement, these values should be considered to be the same.

Table F-1. System Parameters for the Victim Receiver and Calibration Subsystems

	Noise Figure (dB)	Gain (dB)	Input 1-dB Compression Point (Average Power; dBm)	Output 1-dB Compression Point (Average Power; dBm)	Output 1-dB Compression Point (mV <sub>peak</sub> )
Interference Signal Path	18.7	34.9	-35.3	-1.4	269.2
Satellite Signal Path	9.3	44.5	-44.8	-1.3	272.3

Magnitude of the system frequency response was measured by injecting a CW input signal that is incrementally increased in frequency in discrete steps (from 3770 MHz to 3870 MHz) into directional coupler DCPL-1 and measuring the output (at the input to the VSA) with a spectrum analyzer (SA), which tracked the CW input signal in zero-span mode. Both the CW signal generator and the SA operated under computer control to perform this measurement.

Measurements of both the interference and satellite signal paths are shown in Figures F-1 and F-2. Figure F-1 shows system gain over a 100-MHz bandwidth, which is dominated by the 40-MHz, 1-dB bandpass filter (BPF1 in Figure 20). Note that the interference signal path has approximately 10 dB less gain than the satellite signal path due to attenuation in the directional coupler. Figure F-2 shows system gain over the 40-MHz passband of BPF1 at higher resolution. Note that the flatness over the passband for the entire signal path is approximately  $\pm 0.75$  dB.

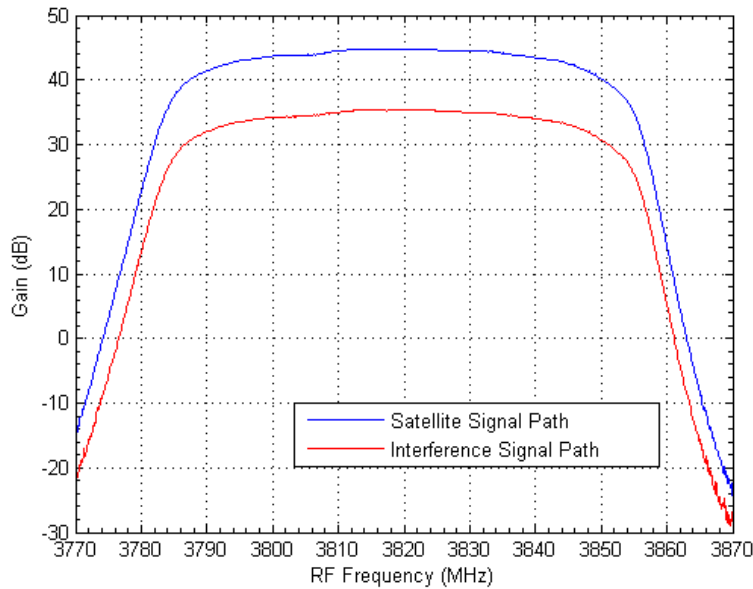


Figure F-1. Frequency response of signal paths.

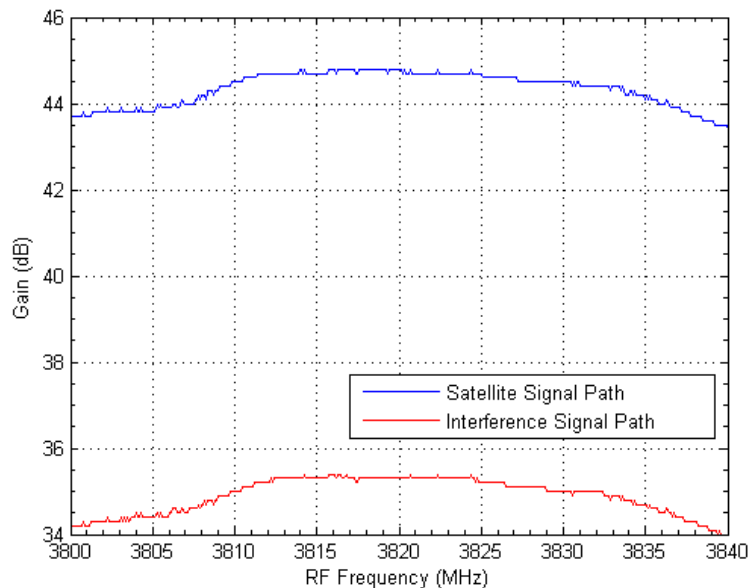


Figure F-2. Passband response of signal paths.

## F.2. Dynamic Range of Interference Signal Path Cascaded with the VSA

During calibration measurements in the DTV interference susceptibility test, the VSA is used to measure interference signals at the output of the interference signal path. It is important to ensure that these measurements are performed at signal levels that do not compress the LNB or the VSA, but are high enough above the noise floor so that lower amplitudes are accurately measured.

Dynamic range measurements, similar to those described in Section E.1, are displayed in Figure F-3. The input range of the VSA was selected to be -10 dBm. Dynamic range of the interference signal path cascaded with the VSA, defined by the straight portion of the CW curve, is approximately 34 dB. In the bandwidth of the VSA, peak-to-average ratios of interference signals do not exceed 25 dB. Setting the average power of these signals to 25 dB below the top of the dynamic range eliminated compression effects and provided a 9-dB margin to accurately measure low amplitudes within the signal.

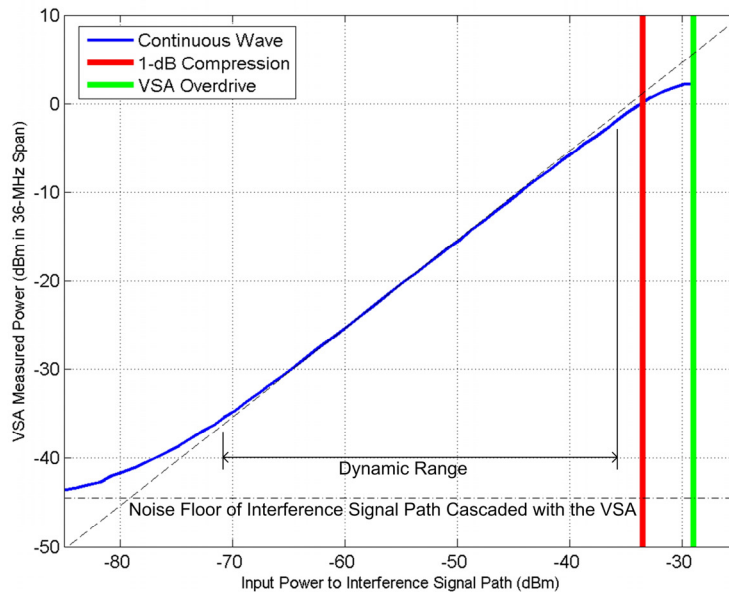


Figure F-3. Dynamic range of the interference signal path cascaded with the VSA.

## F.3. Intermodulation Products in Satellite Signal Generator

As a part of the satellite signal simulator shown in Figure 17, the upconverter frequency shifts the satellite signal from the modulator intermediate frequency of 70 MHz to the satellite channel center frequency of 3820 MHz. Shifting is done in two “mixer” stages. In the first stage, the 1260-MHz local oscillator (LO) frequency produces lower and upper sideband signals centered at 1190 and 1330 MHz. Bandpass filter BPF3 passes the upper sideband signal to the second stage whose 5150-MHz LO frequency produces lower and upper sidebands centered at 3820 and 6480 MHz. Bandpass filter BPF1 in the coupling subsystem (see Figure 20) passes the lower sideband to the LNB.

Practical mixer components, represented by mixer-1 and mixer-2 in Figure F-4, create higher-order intermodulation (IM) products along with the desired frequency conversion products. Figures F-5 and F-6 show the theoretical frequency and corresponding order of these products for the two mixing stages. The 70-MHz intermediate frequency (IF) signal at the input of mixer-1 is depicted by the only first-order, black-horizontal line in Figure F-5. It is 36-MHz wide, which is large compared to the 19.51-MHz wide DTV signal actually being used for testing. Mixing the IF signal with a 1260-MHz LO (shown as a red circle) produces multiple mixing products depicted by the black-horizontal lines at IM orders greater than one. The desired frequency conversion product of the first stage is the upper-sideband signal centered at 1330 MHz, which lies in the passband of bandpass filter BPF3 and is the IF for the second mixing stage (illustrated by the only first-order, black-horizontal line in Figure F-6). High-order mixing products of the second mixing stage are attenuated by BPF1 (shown in Figure 20). Notice that for both mixing stages there are no mixing products below tenth order that lie within the 36-MHz passband of the satellite signal path (bounded by the blue-vertical-dashed lines) – i.e. no higher-order mixing products overlap the desired frequency conversion products. Therefore, the simulated satellite signal centered at 3820 MHz is uncorrupted by higher-order IM products.

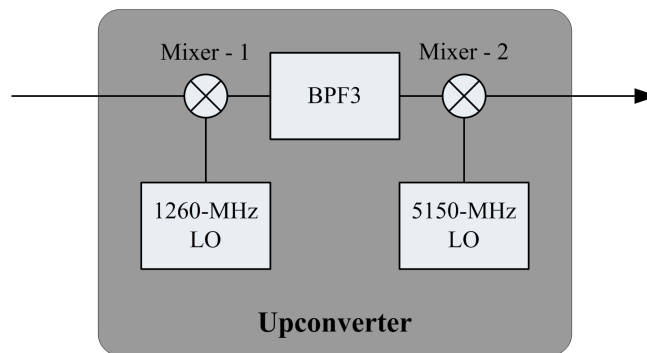


Figure F-4. Upconverter block diagram. Hardware is given in Appendix G.

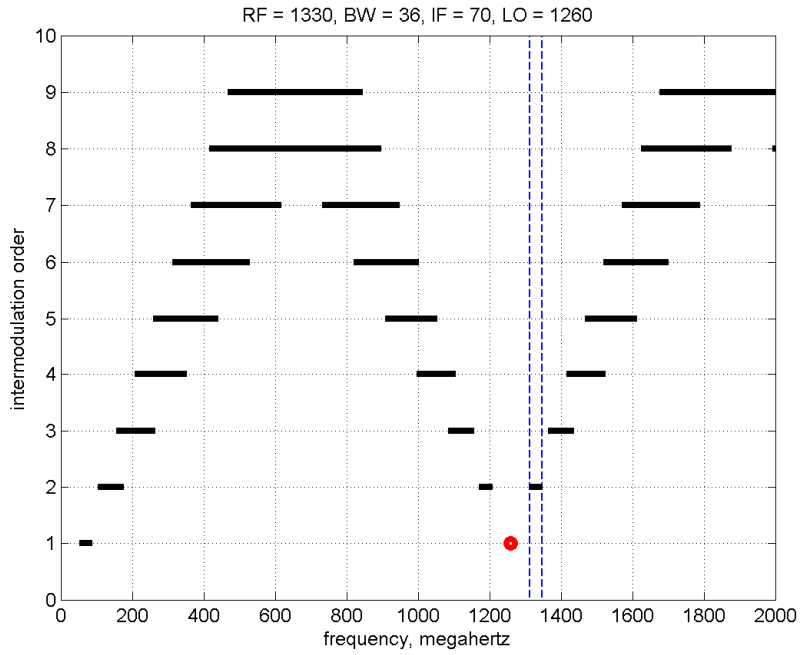


Figure F-5. IM products due to the first mixing stage of the satellite signal generator.

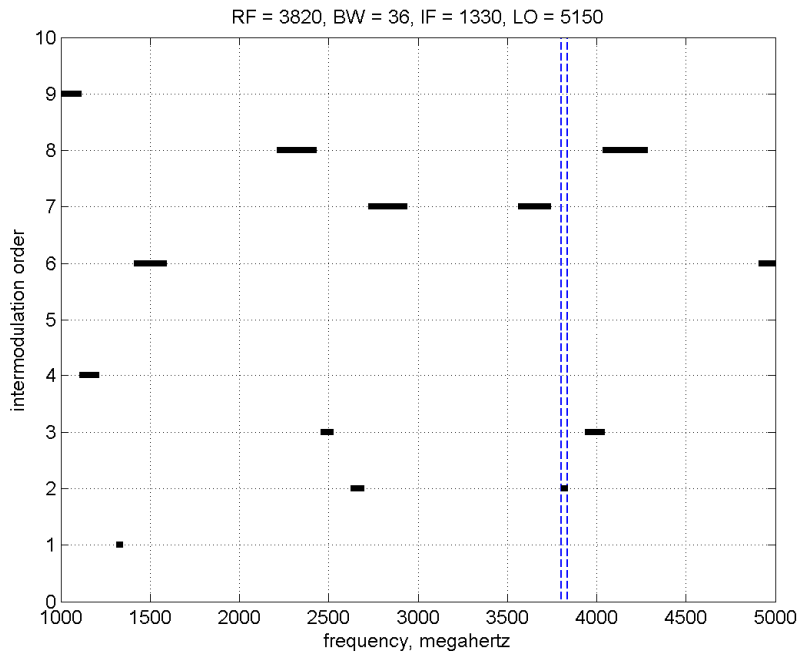


Figure F-6. IM products due to the second mixing stage of the satellite signal generator.

## APPENDIX G: HARDWARE SPECIFICATION

### G.1. Interference Generation Subsystem

Amp (Figure C-2) = Amplifier

Manufacturer: Unknown

Model: 3742-3-35

Serial: 1108

Gain: 38 dB

Frequency Range: 3.7 – 4.2 GHz

AWG (Figure C-2) = Arbitrary Waveform Generator

Manufacturer: Agilent

Model: 33250A

BPF4 (Figure C-2) = Bandpass Filter

Manufacturer: Microwave Filter Co.

Model: 7892-SMA-A

Frequency Range: 3.7 – 4.2 GHz

DCPL - 2 (Figure C-2) = Directional Coupler

Manufacturer: Norsal Ind.

Model: 4871-10

Frequency Range: 0.2 – 18 GHz

Gating Switch (Figure C-2)

Manufacturer: Mini-Circuits

Model: ZASWA-2-50DR

Frequency Range: dc – 5 GHz

Switching Time: 5 ns (typical), 15 ns (maximum)

Noise Diode (Figure C-2)

Manufacturer: Noise/Com, Inc.

Model: NC3208A

Serial: E804

Frequency Range: 0.1-18 GHz

ENR = 27 dB

Signal Generator (Figure C-2)

Manufacturer: Agilent

Model: E8267C option 520 (VSG)

Frequency Range: 250 kHz – 20 GHz

Resolution: 0.001 Hz CW, 0.001 Hz all sweep modes

Switching Speed: < 12 ms typical

Variable Attenuator (Figure C-2)

Manufacturer: Hewlett Packard

Model: HP 8494H and HP 8496B

Frequency Range: 0 – 18 GHz

Attenuation Range: 0 – 11 dB at 1-dB step and 0 – 110 dB at 10-dB step

Variable Attenuator (Figure C-2)

Manufacturer: Narda Microwave

Model: 791 FM

Frequency Range: 2 – 12.4 GHz

Attenuation Range: 0 – 40 dB

VSG (Figures 13, 20, and B-1) = Vector Signal Generator

Manufacturer: Agilent

Model: E8267C option 520

Frequency Range: 250 kHz – 20 GHz

Resolution: 0.001 Hz CW, 0.001 Hz all sweep modes

Switching Speed: < 12 ms typical

## **G.2. Calibration Subsystem/Test and Measurement Equipment**

BPF2 (Figure 20) = Bandpass Filter (tunable)

Manufacturer: K&L Microwave

Model: 5BT-750/1500-5N/N

Serial: 82-9839

Frequency Range: 750 - 1500 MHz

Percentage Bandwidth: 5%

Oscilloscope (Figure 16) – Digital Phosphor Oscilloscope

Manufacturer: Tektronix

Model: TDS7704B

Hardware Analog Bandwidth: 7 GHz

Rise Time: 62 ps 10% to 90% (typical)

Memory: 1 MByte (standard)

Power Divider (Figure 20)

Manufacturer: Midwest Microwave

Model: PWD-5520-03-SMA-79

Frequency Range: 0.5 – 2.0 GHz

Isolation: 15 dB typical

VSWR: 1.5:1

Power Meter (Figure 20)

Manufacturer: Agilent

Model: E4419B

Frequency Range: 9 kHz – 110 GHz, sensor dependent

Power Range: -70 to +44 dBm, sensor dependent

Power Meter Sensor (Figure 20)

Manufacturer: Agilent

Model: E9300A

Frequency Range: 10 MHz – 18 GHz

Power Range: -60 to +20 dBm

Spectrum Analyzer (Figures 15 and 20)

Manufacturer: Agilent

Model: E4440A

Frequency Range: DC – 26.5 MHz

Maximum Resolution Bandwidth: 8 MHz

Vector Signal Analyzer (Figures 14 and 20)

Manufacturer: Agilent

Model: 89641A

Frequency Range: DC – 6 GHz

IF Sample Rate: 95 MS/s

### **G.3. Satellite Simulation Subsystem**

1260-MHz LO (Figure F-4) = Signal Generator

Manufacturer: Hewlett-Packard

Model: HP83413

Frequency Range: 10 MHz – 20 GHz

5150-MHz LO (Figure F-4) = Signal Generator

Manufacturer: Hewlett-Packard

Model: HP 8672A

Frequency Range: 2 GHz – 18 MHz

A1 (Figure 20) – Attenuator

Attenuator/switch driver (Figure 20)

Manufacturer: Agilent

Model: 11713A

BPF3 (Figure F-4) = Bandpass Filter (tunable)

Manufacturer: K&L Microwave

Model: 5BT-750/1500-5N

Serial: 8913-1

Frequency Range: 750 – 1500 MHz

Percentage Bandwidth: 5%

Digital Video Stream (Figure 19) – PCI-Bus Board for Uncompressed Audio/Video Recording

Manufacturer: DVS

Model: ClipStationPRO

Mixer – 1 (Figure F-4) = Frequency Mixer

Manufacturer: Mini-Circuits

Model: ZFM-2000

LO/RF Frequency Range: 100 – 2000 MHz

IF Frequency Range: DC – 600 MHz

Maximum Conversion Loss: 9.5 dB

Minimum LO/RF Isolation: 20 dB

Mixer – 2 (Figure F-4) = Frequency Mixer

Manufacturer: Mini-Circuits

Model: ZX05-C60

LO/RF Frequency Range: 1600 – 6000 MHz

IF Frequency Range: DC – 2000 MHz

Maximum Conversion Loss: 8.3 dB

Minimum LO/RF Isolation: 23 dB (typical), 17 dB (minimum)

Modulator (Figure 19)

Manufacturer: ComTech EF Data

Model: SDM-2020

MPEG-2 Encoder (Figure 19)

Manufacturer: Motorola

Model: SE-1000

Input: analog or digital

Output: DVB-ASI, DHEI, or DS3

Switch – 1 (Figure 20)

Manufacturer: Dow-Key Microwave

Model: 401-2308

Frequency Range: 0 – 26.5 GHz

RF Circuit: SPDT

VA (Figure 20) = Step Variable Attenuator

Manufacturer: Hewlett Packard

Model: HP 8494H and HP 8496B

Frequency Range: 0 – 18 GHz

Attenuation Range: 0 – 11 dB at 1-dB step and 0 – 110 dB at 10-dB step

#### **G.4. Coupling Subsystem**

BPF1 (Figure 20) = Bandpass Filter

Manufacturer: TTE

Model: 310-3820M-40M-A

Center Frequency: 3820 MHz

1-dB Bandwidth: 40 MHz

50-dB Bandwidth: 110 MHz

Insertion Loss:  $\leq 4$  dB

VSWR: 1.5:1

DCPL – 1 (Figure 20) = Directional Coupler

Manufacturer: Narda.

Model: 4202B-10

Frequency Range: 1 – 12.4 GHz

Coupling: 10 dB

Insertion Loss: 1.3 dB (maximum)

Directivity: 15 dB for 1 – 8 GHz, 12 dB for 8 – 12 GHz

VSWR: 1.35

LPF (Figure 20) = Low-pass Filter

Manufacturer: TTE

Model: LMC11-7G-A

3-dB Maximum Frequency: 7 GHz

50-dB Minimum Frequency: 13 – 20 GHz

Insertion Loss:  $\leq 0.2$  dB

VSWR: 1.5:1

## G.5. Receiver Subsystem

### Bias Tee (Figure 20)

Manufacturer: Orbital  
Model: BT1-V2-F-S-B-B  
Frequency Range: 900 – 2100 MHz  
Insertion Loss: 0.5 dB  
Passband Ripple: 0.3 dB (maximum)  
VSWR: 1.3:1  
LNB Interface: 75 $\Omega$  F-type  
Receiver Interface: 50 $\Omega$  SMA

### LNB (Figure 20) – LNA plus Block Downconverter

Manufacturer: Norsat International, Inc.  
Model: 3120 C-band PLL LNB  
Input Frequency Range: 3.4 – 4.2 GHz  
LO Freq: 5.15 GHz  
Stability: +/- 5 kHz  
Noise Temperature = 20 K  
Gain: 60 dB

### MPEG-2 Stream Monitor (Figure 20)

Manufacturer: Tektronix  
Model: MTM400

### Satellite Receiver (Figure 20)

Manufacturer: Motorola/General Instrument  
Model: DSR4500 NTSC

### Switch - 2 (Figure 20)

Manufacturer: Dow-Key Microwave  
Model: 401-2308  
Frequency Range: 0 – 26.5 GHz  
RF Circuit: SPDT

### ZM (Figure 20) = 50 $\Omega$ /75 $\Omega$ Impedance Matching Pad

Model: 9086-50/75  
Power: 1 W  
Frequency: 3 GHz  
Maximum VSWR: 1.25:1  
Insertion Loss: 5.7 dB

## APPENDIX H: GLOSSARY

ADC	analog-to-digital converter
ALC	automatic level control
<i>APD</i>	amplitude probability distribution
AWG	arbitrary waveform generator
BER	bit error rate (italicized <i>BER</i> denotes measured pre-Viterbi bit error rate)
BPF	band-pass filter
BPSK	binary phase-shift keying
CBB	complex baseband
CRADA	cooperative research and development agreement
CS	carrier suppression
CW	continuous wave
DAC	digital-to-analog converter
dB	decibel
dBm	decibel referenced to 1 milliwatt
dBV	decibel referenced to 1 volt
dBW	decibel referenced to 1 watt
DCPL	directional coupler
DO	digital oscilloscope
DP-UWB	dithered-pulse ultrawideband
DS-UWB	direct-sequence ultrawideband
DTV	digital television
DVB	digital video broadcast
ETSI	European Telecommunications Standards Institute
<i>EVM</i>	error vector magnitude
FEC	forward error correction
FCC	Federal Communications Commission
FIR	finite impulse response
FTP	file transfer protocol
GHz	gigahertz = $10^9$ cycles per second
GN	Gaussian noise
GSps	$10^9$ samples per second
I	in-phase
IF	intermediate frequency
IEEE	Institute of Electrical and Electronics Engineers, Inc.
IM	intermodulation
IRD	integrated receiver decoder
ITS	Institute for Telecommunication Sciences
ITU	International Telecommunication Union
LNB	low-noise block downconverter
ln	natural logarithm
LO	local oscillator
log	base-10 logarithm
LPF	low-pass filter
LSB	least significant byte

MAC	medium access control
MB-OFDM	multi-band orthogonal frequency-domain multiplex
MBOA-SIG	MB-OFDM Alliance Special Interest Group
Mbps	million bits per second
<i>MER</i>	modulation error rate
MHz	megahertz = million cycles per second
MPEG	Motion Picture Experts Group
MSB	most significant byte
MSps	million samples per second
ns	nanosecond = $10^{-9}$ seconds
NTIA	National Telecommunications and Information Administration
P/A	peak-to-average ratio
PHY	physical layer
PLCP	physical layer convergence procedure/protocol
PMD	physical medium dependent
PRF	pulse repetition frequency
<i>PSD</i>	power spectral density
Q	quadrature phase
QAM	quadrature amplitude modulating
QPSK	quadrature phase-shift keying
<i>RBW</i>	resolution bandwidth
RF	radio frequency
Rms	root-mean-square
RRC	root-raised cosine
RS	Reed-Solomon
SA	spectrum analyzer
SCPI	Standard Commands for Programmable Instrumentation
<i>SER</i>	segment error rate
SMPTE	Society of Motion Picture and Television Engineers
<i>SNR</i>	signal-to-noise ratio
<i>TEF</i>	transport error flag
UPS	uniform pulse spacing
UTC	coordinated universal time
UWB	ultrawideband
V	volt
VA	variable attenuator
<i>VBW</i>	video bandwidth
VSA	vector signal analyzer
VSG	vector signal generator
WLAN	wireless local area network
WPAN	wireless personal area network